PMC Physics A

PhysMath Central

Research article

Open Access

Semi-analytical approach to magnetized temperature autocorrelations

Massimo Giovannini

Address: Centro "Enrico Fermi", Via Panisperna 89/A, 00184 Rome, Italy
Department of Physics, Theory Division, CERN, 1211 Geneva 23, Switzerland

Email: Massimo Giovannini - massimo.giovannini@cern.ch

Published: 18 October 2007

PMC Physics A 2007, **1**:5 doi:10.1186/1754-0410-1-5

Received: 18 October 2007
Accepted: 18 October 2007

This article is available from: http://www.physmathcentral.com/1754-0410/1/5

Abstract

The cosmic microwave background (CMB) temperature autocorrelations, induced by a magnetized adiabatic mode of curvature inhomogeneities, are computed with semi-analytical methods. As suggested by the latest CMB data, a nearly scale-invariant spectrum for the adiabatic mode is consistently assumed. In this situation, the effects of a fully inhomogeneous magnetic field are scrutinized and constrained with particular attention to harmonics which are relevant for the region of Doppler oscillations. Depending on the parameters of the stochastic magnetic field a hump may replace the second peak of the angular power spectrum. Detectable effects on the Doppler region are then expected only if the magnetic power spectra have quasi-flat slopes and typical amplitude (smoothed over a comoving scale of Mpc size and redshifted to the epoch of gravitational collapse of the protogalaxy) exceeding 0.1 nG. If the magnetic energy spectra are bluer (i.e. steeper in frequency) the allowed value of the smoothed amplitude becomes, comparatively, larger (in the range of 20 nG). The implications of this investigation for the origin of large-scale magnetic fields in the Universe are discussed. Connections with forthcoming experimental observations of CMB temperature fluctuations are also suggested and partially explored.

1 Formulation of the problem

Since the Cosmic Microwave Background (CMB) is extremely isotropic in nearly all angular scales, it is rather plausible to infer that the Universe was quite homogeneous (and isotropic) at the moment when the ionization fraction dropped significantly and the photon mean free path became, almost suddenly, comparable with the present Hubble radius.

The inhomogeneities present for length-scales larger than the Hubble radius right before recombination are believed to be, ultimately, the seeds of structure formation and they can be studied by looking at the temperature autocorrelations which are customarily illustrated in terms of the angular power spectrum. The distinctive features of the angular power spectrum (like the

Doppler peaks) can be phenomenologically reproduced by assuming the presence, before recombination, of a primordial adiabatic [2]mode arising in a spatially flat Universe [1-5]. Possible deviations from this working hypothesis can also be bounded: they include, for instance, the plausible presence of non-adiabatic modes (see [6-8] and references therein), or even features in the power-spectrum that could be attributed either to the pre-inflationary stage of expansion or to the effective modification of the dispersion relations (see [9-12] and references therein). For a pedagogical introduction to the physics of CMB anisotropies see, for instance, Ref. [13]. In short the purpose of the present paper is to show that CMB temperature autocorrelations may also be a source of valuable informations on large-scale magnetic fields whose possible presence prior to recombination sheds precious light on the origin of the largest magnetized structures we see today in the sky such as galaxies, clusters of galaxies and even some supercluster.

In fact, spiral galaxies and rich clusters possess a large-scale magnetic field that ranges from 500 nG [14,15] (in the case of Abell clusters) to few μG in the case of spiral galaxies [16]. Elliptical galaxies have also magnetic fields in the μG range but with correlation scales of the order of 10–100 pc (i.e. much smaller than in the spirals where typical correlation lengths are of the order of 30 kpc, as in the case of the Milky Way). The existence of large-scale magnetic fields in superclusters, still debatable because of ambiguities in the determination of the column density of electrons along the line of sight, would be rather intriguing. Recently plausible indications of the existence of magnetized structures in Hercules and Perseus-Pisces superclusters have been reported [17] (see also [18]): the typical correlation scales of the fields would be 0.5 Mpc and the intensity 300 nG.

While there exist various ideas put forward throught the years, it is fair to say that the origin of these (pretty large) fields is still matter of debate [15,19]. Even if they are, roughly, one millionth of a typical planetary magnetic field (such as the one of the earth) these fields are pretty large for a cosmological standard since their energy density is comparable both with energy density of the CMB photons (i.e. $T_{\rm CMB}^4$) and with the cosmic ray pressure. The very presence of large scale magnetic fields in diffuse astrophysical plasmas and with large correlation scales (as large of, at least, 30 kpc) seems to point towards a possible primordial origin [15]. At the same time, the efficiency of dynamo amplification can be questioned in different ways so that, at the onset of the gravitational collapse of the protogalaxy it seems rather plausible that only magnetic fields with intensities[3] $B_{\rm L} > 10^{-14}$ nG may be, eventually, amplified at an observable level [20,21].

As emphasized many years ago by Harrison [22-24], this situation is a bit reminiscent of what happened with the problem of justifying the presence of a flat spectrum of curvature perturbations that could eventually seed the structure formation paradigm. Today a possibility along this direction is provided by inflationary models in one of their various incarnations.

It seems therefore appropriate, especially in view of forthcoming satellite missions (like PLANCK Explorer [25]), to discuss the effects of large-scale magnetic fields on CMB physics. In fact, all along the next decade dramatic improvements in the quality and quantity of CMB data can be expected. On the radio-astronomical side, the next generation of radio-telescopes such as Square Kilometre Array (SKA) [26] might be able to provide us with unprecedented accuracy in the full sky survey of Faraday Rotation measurements at frequencies that may be so large to be, roughly, comparable with [4] (even if always smaller than) the lower frequency channel of the PlANCK Explorer (i.e. about 30 GHz). The question before us today is, therefore, the following: is CMB itself able to provide compelling bounds on the strength of large-scale magnetic fields prior to hydrogen recombination? In fact, all the arguments connecting the present strength of magnetic field to their primordial value (say before recombination) suffer undeniable ambiguities. These ambiguities are related to the evolution of the Universe through the dark ages (i.e. approximately, between photon decoupling and galaxy formation). So, even if it is very reasonable to presume that during the stage of galaxy formation the magnetic flux and helicity are, according to Alfvén theorems, approximately conserved, the strengths of the fields prior to gravitational collapse is unknown and it is only predictable within a specific model for the origin of large-scale magnetic fields. In general terms, the magnetic fields produced in the early Universe may have different features. They may be helical or not, they may have different spectral slopes and different intensities. There are, however, aspects that are common to diverse mechanisms like the stochastic nature of the produced field. Furthermore, since as we go back in time the conductivity increases with the temperature, it can be expected that the flux freezing and the helicity conservation are better and better verified as the Universe heats up say from few eV to few MeV.

Along the past decade some studies addressed the analysis of vector and tensor modes induced by large-scale magnetic fields [28-31]. There have been also investigations within a covariant approach to perturbation theory [32,33]. Only recently the analysis of the scalar modes has been undertaken [34-38]. The set-up of the aforementioned analyses is provided by an effective one-fluid description of the plasma which is essentially the curved space analog of magnetohydrodynamics (MHD). This approach is motivated since the typical length-scales of the problem are much larger of the Debye length. However, it should be borne in mind that the treatment of Faraday rotation is a typical two-fluid phenomenon. So if we would like to ask the question on how the polarization plane of the CMB is rotated by the presence of a uniform magnetic field a two-fluid description would be mandatory (see section 2 and references therein).

In the framework described in the previous paragraph, it has been shown that the magnetic fields affect the scalar modes in a threefold way. In the first place the magnetic energy density and pressure gravitate inducing a computable modification of the large-scale adiabatic solution. Moreover, the anisotropic stress and the divergence of the Lorentz force affect the evolution of the baryon-lepton fluid. Since, prior to decoupling, photons and baryons are tightly coupled the

net effect will also be a modification of the temperature autocorrelations at angular scales smaller than the ones relevant for the ordinary SW contribution (i.e. $\ell > 30$).

In the present paper, elaborating on the formalism developed in [34-36], a semi-analtytical approach for the calculation of the temperature autocorrelations is proposed. Such a framework allows the estimate of the angular power spectrum also for angular scales compatible with the first Doppler peak. A gravitating magnetic field will be included from the very beginning and its effects discussed both at large angular scales and small angular scales. The main theme of the present paper can then be phrased by saying that large-scale magnetic fields affect the geometry and the evolution of the (scalar) sources. We ought to compute how all these effects combine in the final power spectra of the temperature autocorrelations. It should be remarked, incidentally, that the evolution of the density contrasts of the various species enter directly the scalar problem but neither the vector or the tensor modes are affected by their presence. As a consequence of this occurrence the self-consistent inclusion of the large-scale magnetic fields in the calculation is much more cumbersome than in the case of the tensor and vector modes.

The plan of the present paper will therefore be the following. In section 2 the typical scales of the problem will be discussed. In section 3 the attention will be focused on the large-scale evolution of the curvature perturbations with particular attention to the magnetized contribution, i.e. the contribution associated with the gravitating magnetic fields. In section 4 the evolution at smaller angular scales will be investigated accounting, in an approximate manner, for the finite thickness effects of the last-scattering surface. In section 5 the estimates of the angular power spectra of the temperature autocorrelations will be presented. Section 6 contains the concluding remarks. Some of the relevant theoretical tools needed for the discussion of the problem have been collected in the appendix with the sole aim to make the overall presentation more self-contained. The material presented in the appendix collects the main equations whose solutions are reported and discussed in section 3 and 4.

2 Typical scales of the problem

The analysis starts by defining all the relevant physical scales of the problem. These scales stem directly from the evolution equations of the gravitational perturbations in the presence of a stochastic magnetic field. The interested reader may also consult appendix A where some relevant technical aspects are briefly summarized.

2.1 Equality and recombination

According to the present understanding of the Doppler oscillations the space-time geometry is well described by a conformally flat line element of Friedmann-Robertson-Walker (FRW) type

$$ds^2 = a^2(\tau)[d\tau^2 - d\vec{x}^2], \tag{2.1}$$

where t is the conformal time coordinate. In the present paper the general scheme will be to introduce the magnetic fields in the standard lore where the space-time geometry is spatially flat. This is the first important assumption which is supported by current experimental data including the joined analysis of, at least, three sets of data stemming, respectively from large-scale structure, from Type Ia supernovae and from the three year WMAP data (eventually combined with other CMB experiments). For the interpretation of the data a specific model must also be adopted. The framework of the present analysis will be the one provided by the ΛCDM model. This is probably the simplest case where the effects of magnetic fields can be included. Of course one may also ask the same question within a different underlying model (such as the open CDM model or the ΛCDM model with sizable contribution from the tensor modes and so on and so forth). While the calculational scheme will of course be a bit different, the main logic will remain the same. More details on the typical values of cosmological parameters inferred in the framework of the ΛCDM model can be found at the beginning of section 5.

In the geometry given by Eq. (2.1) the scale factor for the radiation-matter transition can be smoothly parametrized as

$$a(\tau) = a_{\rm eq}\left[\left(\frac{\tau}{\tau_1}\right)^2 + 2\left(\frac{\tau}{\tau_1}\right)\right], \quad \tau_1 = \frac{2}{H_0}\sqrt{\frac{a_{\rm eq}}{\Omega_{\rm M0}}} \simeq 288\left(\frac{h_0^2\Omega_{\rm M0}}{0.134}\right)^{-1}\ {\rm Mpc}. \tag{2.2}$$

Concerning Eqs. (2.1) and (2.2) few comments are in order:

• the conformal time coordinate is rather useful for the treatment of the evolution of magnetized curvature perturbations and is extensively employed in the appendix A;

• H_0 is the present value of the Hubble constant and $\Omega_{\rm M0}$ is the present critical fraction in non-relativistic matter, i.e. $\Omega_{\rm M0} = \Omega_{\rm b0} + \Omega_{\rm c0}$, given by the sum of the CDM component and of the baryonic component;

• in the notation of Eq. (2.2) the equality time (i.e. the time at which the radiation contribution equals the contribution of dusty matter) is easily determined to be $\tau_{\rm eq} = (\sqrt{2} - 1)\tau_1$, i.e. roughly, $\tau_{\rm eq} \simeq \tau_1/2$.

Equation (2.2) is a solution of the Friedmann-Lemaître equations whose specific form is

$$\mathcal{H}^2 = \frac{8\pi G}{3}a^2\rho_{\rm t}, \tag{2.3}$$

$$\mathcal{H}^2 - \mathcal{H}' = 4\pi G a^2 (\rho_{\rm t} + p_{\rm t}), \tag{2.4}$$

$$\rho_{\rm t}' + 3\mathcal{H}(\rho_{\rm t} + p_{\rm t}) = 0, \tag{2.5}$$

where $\mathcal{H} = a'/a$ and the prime will denote, throughout the paper, a derivation with respect to τ. Equation (2.2) is indeed solution of Eqs. (2.3), (2.4) and (2.5) when the total energy density $\rho_{\rm t}$ is given by the sum of the matter density $\rho_{\rm M}$ and of the radiation density $\rho_{\rm R}$ (similarly $p_{\rm t} = p_{\rm R} + p_{\rm M}$).

Often, for notational convenience, the rescaled time coordinate $x = \tau/\tau_1$ will be used. Within this x parametrization the critical fractions of radiation and dusty matter become

$$\Omega_{\rm R}(x) = \frac{1}{\alpha(x)+1} = \frac{1}{(x+1)^2}, \quad \Omega_{\rm M}(x) = \frac{\alpha(x)}{\alpha(x)+1} = \frac{x^2+2x}{(x+1)^2}. \tag{2.6}$$

The redshift to equality is given, from Eq. (2.2), by

$$z_{\rm eq} + 1 \simeq \frac{\rho_{\rm M0}}{\rho_{\rm R0}} = \frac{h_0^2 \Omega_{\rm M0}}{h_0^2 \Omega_{\rm R0}} = 3228.91 \left(\frac{h_0^2 \Omega_{\rm M0}}{0.134} \right). \tag{2.7}$$

The redshift to recombination $z_{\rm rec}$ is, approximately, between 1050 and 1150. From this hierarchy of scales, i.e. $z_{\rm dec} > z_{\rm rec}$, it appears that recombination takes place when the Universe is already dominated by matter. Furthermore, a decrease in the fraction of dusty matter delays the onset of the matter dominated epoch.

If the recombination happens suddenly, the ionization fraction $x_{\rm e}$ drops abruptly from 1 to 10^{-5}. Prior to recombination the photons interact with protons and electrons via Thompson scattering so that the relevant mean free path is, approximately,

$$\lambda_{\rm T}(z_{\rm rec}) \simeq \frac{1.8}{x_{\rm e}} \left(\frac{0.023}{h_0^2 \Omega_{\rm b0}} \right) \left(\frac{1100}{1+z_{\rm rec}} \right)^2 \left(\frac{0.88}{1 - Y_{\rm p}/2} \right) {\rm Mpc}, \tag{2.8}$$

where $Y_{\rm p} \simeq 0.24$ is the abundance of ^{4}He. Since $m_{\rm p} = 0.938$ GeV and $m_{\rm e} = 0.510$ MeV, the mean free path of the photons will be essentially determined by the electrons because the Thompson cross section is smaller for protons than for electrons. Furthermore the protons and the electrons are even more tightly coupled, among them, by Coulomb scattering whose rate is larger than the Thompson rate of interaction. When the ionization fraction drops the photon mean free path gets as large as 10^4 Mpc. For the purposes of this investigation it will be also important to take

into account, at least approximately, the finite thickness of the last scattering surface. This can be done by approximating the visibility function with a Gaussian profile [39-43](see also [44,45]) with finite width. We recall that the visibility function simply gives the probability that a photon was last scattered between τ and $\tau + d\tau$ (see section 4). The scale factor (2.2) can be used to express the ratios of two typical time-scales in terms of the ratio between the corresponding redshifts. So, for instance,

$$x_{\rm rec} = \frac{\tau_{\rm rec}}{\tau_1} = \sqrt{\frac{z_{\rm eq}+1}{z_{\rm rec}+1} + 1} - 1, \tag{2.9}$$

which implies that, for $z_{\rm rec}$ and $h_0^2\Omega_{\rm M0} = 0.134$, $\tau_{\rm rec} = 1.01\,\tau_1$.

There is another typical scale that plays an important role in the discussion of the Doppler oscillations. It is the baryon to photon ratio and it is defined as

$$R_{\rm b}(z) = \frac{3}{4}\frac{\rho_{\rm b}}{\rho_\gamma} = 0.664\left(\frac{h_0^2\Omega_{\rm b0}}{0.023}\right)\left(\frac{1051}{z+1}\right). \tag{2.10}$$

In the treatment of the angular power spectrum at intermediate angular scales $R_{\rm b}(z)$ appears ubiquitously either alone or in the expression of the sound speed of the photon-baryon system (see appendix A for further details)

$$c_{\rm sb}(z) = \frac{1}{\sqrt{3(R_{\rm b}(z)+1)}}. \tag{2.11}$$

In the absence of a magnetized contribution, $R_{\rm b}(z_{\rm rec})$ sets the height of the first Doppler peak as it can be easily argued by solving the evolution of the photon density contrast in the WKB approximation (see Eqs. (A.34) and (A.35)).

2.2 Plasma scales

The Debye scale and the plasma frequency of the electrons can be easily computed in terms of the cosmological parameters introduced so far. The results are, respectively:

$$\lambda_{\rm D}(z) = \sqrt{\frac{T_{\rm e}}{8\pi e^2 n_{\rm e}}} \simeq \frac{4.26}{\sqrt{x_{\rm e}}}\left(\frac{1050}{z+1}\right)\left(\frac{h_0^2\Omega_{\rm b0}}{0.023}\right)^{-1/2}\,{\rm cm}, \tag{2.12}$$

$$\omega_{\rm pe}(z) = 3.45\left(\frac{h_0^2\Omega_{\rm b0}}{0.023}\right)^{1/2}\left(\frac{1+z}{1050}\right)^{3/2}\,{\rm MHz}. \tag{2.13}$$

By comparing Eqs. (2.8) and (2.12), $\lambda_{\rm T}\bar{}\,\lambda_{\rm D}$ both around equality and recombination. For typical scales comparable with the Hubble radius at recombination, therefore, the plasma will be, to an excellent approximation, globally neutral, i.e.

$$\vec{\nabla}\cdot\vec{E} = 4\pi e(n_{\rm p} - n_{\rm e}) = 0 \tag{2.14}$$

where $\vec{E}(\tau,\vec{x}) = a^2(\tau)\vec{\mathcal{E}}(\tau,\vec{x})$ denote the rescaled electric fields and where, by charge neutrality, the electron density equals the proton density, i.e.

$$n_{\rm e}(z) = n_{\rm p}(z) = x_{\rm e}\eta_{\rm b}n_\gamma(z), \quad \eta_{\rm b} = 6.27\times10^{-10}\left(\frac{h_0^2\Omega_{\rm b0}}{0.023}\right); \tag{2.15}$$

$\eta_{\rm b}$ is the ratio between the baryonic charge density and the photon density. When the ionization fraction drops, the Debye scale is still the smallest length of the problem. From Eq. (2.13) the plasma frequency for the electrons is, around recombination, in the MHz range. The plasma frequency for the ions (essentially protons) will then be smaller (in the kHz range). Both these frequencies are smaller than the maximum of the CMB emission (which is, today, around 300 GHz and around 300 THz around recombination). Since the main focus of the present investigation will be on frequencies $\omega << \omega_{\rm pe}$, the electromagnetic propagation of disturbances can be safely neglected and this implies, in terms of the rescaled electric and magnetic fields, that

$$\vec{\nabla}\times\vec{B} = 4\pi\vec{J}, \quad \vec{\nabla}\cdot\vec{B} = 0 \tag{2.16}$$

where $\vec{B}(\tau,\vec{x}) = a^2\vec{\mathcal{B}}(\tau,\vec{x})$ and where

$$\vec{J} = \sigma_{\rm c}(\vec{E} + \vec{v}\times\vec{B}), \tag{2.17}$$

is the Ohmic current and $\sigma_{\rm c} = a(\tau)\ \bar{\sigma}_{\rm c}$ defined in terms of the rescaled conductivity. Since we are in the situation where $T << m_{\rm e}$, $\bar{\sigma}_{\rm c} = \alpha_{\rm em}^{-1}T\sqrt{T/m_{\rm e}}$. By now using the Ohmic electric field inside the remaining Maxwell equation, i.e.

$$\vec{\nabla}\times\vec{E} = -\frac{\partial\vec{B}}{\partial\tau}, \tag{2.18}$$

the magnetic diffusivity equation can be obtained

$$\frac{\partial \vec{B}}{\partial \tau} = \vec{\nabla} \times (\vec{v} \times \vec{B}) + \frac{1}{4\pi\sigma_{\rm c}} \nabla^2 \vec{B}. \tag{2.19}$$

Equation (2.19) together with the previous equations introduced in the present subsection are the starting point of the magnetohydrodynamical (MHD) description adopted in the present paper. They hold for typical frequencies $\omega << \omega_{\rm pe}$ and for typical length scales much larger than the Debye scale. In this approximation (see Eq. (2.16)) the Ohmic current is solenoidal, i.e. $\vec{\nabla} \cdot \vec{J} = 0$.

As in the flat-space case, the MHD equations can be obtained from a two-fluid description by combining the relevant equations and by using global variables. As a consequence of this derivation $\vec{J}$ will be the total current and $\vec{v}$ will be the bulk velocity of the plasma, i.e. the centre-of-mass velocity of the electron-proton system [46,47]. It should be remembered that various phenomena involving the possible existence of a primordial magnetic field at recombination should not be treated within a single fluid approximation (as it will be done here) but rather within a two-fluid (or even kinetic) description. An example along this direction is Faraday rotation of the CMB polarization [48] or any other phenomenon where the electromagnetic branch of the plasma spectrum is relevant, i.e. $\omega > \omega_{\rm pe}$. In fact, the CMB is linearly polarized. So if a uniform magnetic field is present at recombination the polarization plane of the CMB can be rotated. From the appropriate dispersion relations (obtainable in the usual two-fluid description) the Faraday rotation rate can be computed bearing in mind that the Larmor frequency of electrons and ions at recombination, i.e.

$$\omega_{\rm Be} = \frac{e B_{\rm L}(\tau_{\rm rec})}{m_{\rm e} c} \simeq 18.08 \left(\frac{B_{\rm L}(\tau_{\rm rec})}{10^{-3}\,{\rm G}} \right) {\rm kHz}, \quad \omega_{\rm Bi} = \frac{e B_{\rm L}(\tau_{\rm rec})}{m_{\rm i} c} \simeq 9.66 \left(\frac{B_{\rm L}(\tau_{\rm rec})}{10^{-3}\,{\rm G}} \right) {\rm Hz}, \tag{2.20}$$

are both smaller than $\omega_{\rm pe}$. In Eq. (2.20) $B_{\rm L}(\tau_{\rm rec})$ is the smoothed magnetic field strength at recombination.

It is the moment to spell out clearly two concepts that are central to the discussion of the evolution of large-scale magnetic fields in a FRW Universe with line element (2.1):

- the concept of comoving and physical magnetic fields;
- the concept of stochastic magnetic field.

The comoving magnetic field $\vec{B}(\tau,\vec{x})$ is related to the physical magnetic field $\vec{\mathcal{B}}(\tau,\vec{x})$ as $\vec{B}(\tau,\vec{x}) = a^2(\tau)\vec{\mathcal{B}}(\tau,\vec{x})$. We will choose as the reference time the epoch of gravitational collapse of the protogalaxy. At this time the comoving and physical field coincide. So, for instance, a (physical) magnetic field of nG strength at the onset of gravitational collapse will be roughly of the order of the mG (i.e. 10^{-3} G) at the epoch of recombination. This conclusion stems directly from the fact that the physical magnetic field scales with $a^{-2}(\tau)$, i.e. with z^2 where z, as usual is the redshift. This implies, in turn, that $\vec{B}$ (i.e. the comoving field) is roughly constant (in time) if the plasma does not have sizable kinetic helicity[5](i.e. $\langle\vec{v}\cdot\vec{\nabla}\times\vec{v}\rangle = 0$) (see, for instance, [15,20,21]). In this situation Eq. (2.19) dictates that $\vec{B}$ is constant for typical wave-numbers $k < k_\sigma$ (i.e. for sufficiently large comoving length-scales) where k_σ sets the magnetic diffusivity scale whose value, at recombination, is

$$\frac{1}{k_\sigma} \simeq 1.24\times 10^{-14}\left(\frac{h_0^2\Omega_{\rm M0}}{0.134}\right)^{-3/4}\ {\rm Mpc}. \tag{2.21}$$

Equation (2.21) can be compared with the estimate of the diffusive scale associated with Silk damping:

$$\frac{1}{k_{\rm D}\tau_{\rm rec}} = 9.63\times 10^{-3}\left(\frac{h_0^2\Omega_{\rm b}}{0.023}\right)^{-1/2}\left(\frac{h_0^2\Omega_{\rm M}}{0.134}\right)^{1/4}\left(\frac{1050}{z_{\rm rec}}\right)^{3/4}. \tag{2.22}$$

Hence, for the typical value of the matter fraction appearing in Eq. (2.21), $\tau_{\rm rec} \simeq \tau_1$ and, consequently $k_\sigma \bar{} k_{\rm D}$. While finite conductivity effects are rather efficient in washing out the magnetic fields for large wave-numbers, the thermal diffusivity effects (related to shear viscosity and, ultimately, to Silk damping) affect typical wave-numbers that are much smaller than the ones affected by conductivity.

Under the conditions of MHD, two (approximate) conservations laws may be derived, namely the magnetic flux conservation

$$\frac{d}{d\tau}\int_\Sigma \vec{B}\cdot d\vec{\Sigma} = -\frac{1}{4\pi\sigma_{\rm C}}\int_\Sigma \vec{\nabla}\times\vec{\nabla}\times\vec{B}\cdot d\vec{\Sigma}, \tag{2.23}$$

and the magnetic helicity conservation

$$\frac{d}{d\tau}\left(\int_V d^3x\vec{A}\cdot\vec{B}\right) = -\frac{1}{4\pi\sigma_C}\int_V d^3x\ \vec{B}\cdot\vec{\nabla}\times\vec{B}. \tag{2.24}$$

In Eq. (2.23) Σ is an arbitrary closed surface that moves with the plasma. In Eq. (2.24) $\vec{A}$ is the vector potential. According to Eq. (2.23), in MHD the magnetic field has to be always solenoidal (i.e. $\vec{\nabla}\cdot\vec{B}=0$). Thus, the magnetic flux conservation implies that, in the ideal MHD limit (i.e. $\sigma_c\to\infty$) the magnetic flux lines, closed because of the transverse nature of the field, evolve always glued together with the plasma element. In this approximation, as far as the magnetic field evolution is concerned, the plasma is a collection of (closed) flux tubes. The theorem of flux conservation states then that the energetical properties of large-scale magnetic fields are conserved throughout the plasma evolution.

While the flux conservation concerns the energetic properties of the magnetic flux lines, the magnetic helicity, i.e. Eq. (2.24), concerns chiefly the topological properties of the magnetic flux lines. In the simplest situation, the magnetic flux lines will be closed loops evolving independently in the plasma and the helicity will vanish. There could be, however, more complicated topological situations [51] where a single magnetic loop is twisted (like some kind of Möbius stripe) or the case where the magnetic loops are connected like the rings of a chain: now the non-vanishing magnetic helicity measures, essentially, the number of links and twists in the magnetic flux lines [47]. Furthermore, in the superconducting limit, the helicity will not change throughout the time evolution. The conservation of the magnetic flux and of the magnetic helicity is a consequence of the fact that, in ideal MHD, the Ohmic electric field is always orthogonal both to the bulk velocity field and to the magnetic field. In the resistive MHD approximation this conclusion may not apply. The quantity at the right-hand-side of Eq. (2.24), i.e. $\vec{B}\cdot\vec{\nabla}\times\vec{B}$ is called magnetic gyrotropy and it is a gauge-invariant measure of the number of contact points in the magnetic flux lines. As we shall see in a moment, the only stochastic fields contributing to the scalar fluctuations of the goemetry are the ones for which the magnetic gyrotropy vanishes.

Nearly all mechanisms able to generate large scale magnetic fields imply the existence of a stochastic background of magnetic disturbances [15] that could be written, in Fourier space, as [6]

$$\left\langle B_i(\vec{k},\tau)B_j(\vec{p},\tau)\right\rangle = P_{ij}(k)\delta^{(3)}(\vec{k}+\vec{p}), \tag{2.25}$$

where

$$P_{ij}(k) = Q(k)\left(\delta_{ij} - \frac{k_i k_j}{k^2}\right), \quad Q(k) = Q_0 k^m. \tag{2.26}$$

From Eq. (2.26) the magnetic field configuration of Eq. (2.25) depends on the amplitude of the field Q_0 and on the spectral index m.

It is often useful, in practical estimates, to regularize the two-point function by using an appropriate "windowing". Two popular windows are, respectively, the Gaussian and the top-hat functions, i.e.

$$\mathcal{W}_{\rm g}(k,L) = e^{-\frac{k^2L^2}{2}}, \quad \mathcal{W}_{\rm th}(k,L) = \frac{3}{kL} j_1(kL). \tag{2.27}$$

For instance, the regularized magnetic energy density with Gaussian filter can be obtained from the previous expressions by shifting $Q(k) \to Q(k) W_{\rm g}^2(k,L)$. The result is

$$\left\langle B_i(\tau,\vec{x}) B^i(\tau,\vec{x}+\vec{r}) \right\rangle = \frac{2Q_0}{(2\pi)^2} \frac{\Gamma\left(\frac{m+3}{2}\right)}{L^{3+m}} F\left(\frac{m+3}{2}, \frac{3}{2}, -\frac{r^2}{4L^2}\right), \tag{2.28}$$

where $F(a, b, x) \equiv {}_1F_1(a, b, x)$ is the confluent hypergeometric function [52,53]. Notice that the integral appearing in the trace converges for $m > -3$. The amplitude of the magnetic power spectrum Q_0 can be traded for $B_{\rm L}^2$ where $B_{\rm L}^2$ is by definition the regularized two-point function evaluated at coincident spatial points, i.e.

$$B_{\rm L}^2 = \lim_{r\to 0} \left\langle B_i(\tau,\vec{x}) B^i(\tau,\vec{x}+\vec{r}) \right\rangle \tag{2.29}$$

Combining Eq. (2.28) with Eq. (2.29) we have that Q_0 becomes

$$Q_0 = \frac{(2\pi)^{m+5}}{2} \frac{k_{\rm L}^{-(3+m)}}{\Gamma\left(\frac{m+3}{2}\right)} B_{\rm L}^2, \tag{2.30}$$

where $k_{\rm L} = 2\pi/L$. The two main parameters that will therefore characterize the magnetic background will be the smoothed amplitude $B_{\rm L}$ and the spectral slope. For reasons related to the way power spectra are assigned for curvature perturbations, it will be practical to define the magnetic spectral index as $\varepsilon = m + 3$ (see Eqs. (3.40)-(3.41) and comments therein).

In the case of the configuration (2.25) the magnetic gyrotropy is vanishing, i.e. $\langle \vec{B} \cdot \vec{\nabla} \times \vec{B} \rangle = 0$. There are situations where magnetic fields are produced in a state with non-vanishing gyrotropy (or helicity) (see for instance [54] and references therein). In the latter case, the two point function can be written in the same form given in Eq. (2.25)

$$\left\langle B_i(\vec{k},\tau) B_j(\vec{p},\tau) \right\rangle = \tilde{P}_{ij}(k) \delta^{(3)}(\vec{k} + \vec{p}), \tag{2.31}$$

but where now

$$\tilde{P}_{ij}(k) = Q(k) \left(\delta_{ij} - \frac{k_i k_j}{k^2} \right) + i \tilde{Q}(k) \varepsilon_{ij\ell} \frac{k^\ell}{k}, \quad \tilde{Q}(k) = \tilde{Q}_0 k^{\tilde{m}}. \tag{2.32}$$

From Eq. (2.32) we can appreciate that, on top of the parity-invariant contribution (already defined in Eqs. (2.25) and (2.26)), there is a second term proportional to the Levi-Civita $\varepsilon_{ij}\ell$. In Fourier space, the introduction of gyrotropic configurations implies also the presence of a second function of the momentum $\tilde{Q}(k)$. In the case of scalar fluctuations of the geometry this second power spectrum will not give any contribution (but it does contribute to the vector modes of the geometry as well as in the case of the tensor modes).

The correlators that contribute to the evolution of the scalar fluctuations of the geometry will be essentially the ones of magnetic energy density and pressure (i.e. $\vec{B}^2/(8\pi)$ and $\vec{B}^2/(24\pi)$) and the one related to the divergence of the MHD Lorentz force (i.e. $\vec{\nabla} \cdot [\vec{J} \times \vec{B}]$) which appears as source term in the evolution equation of the divergence of the peculiar velocity of the baryons (see Eqs. (A.23) and (A.25) of the appendix A). Since in MHD $4\pi \vec{J} = \vec{\nabla} \times \vec{B}$ the divergence of the Lorentz force will be proportional to $\vec{\nabla} \cdot [(\vec{\nabla} \times \vec{B}) \times \vec{B}]$. The magnetic anisotropic stress $\tilde{\Pi}_i^j$ does also contribute to the scalar problem but it can be related, through simple vector identities, to the magnetic energy density and to the divergence of the Lorentz force (see Eqs. (A.28) and (A.29)). To specify the effect of the stochastic background of magnetic fields on the scalar modes of the geometry we shall therefore need the correlation functions of two dimensionless quantities denoted, in what follows, by $\Omega_{\rm B}$ and $\sigma_{\rm B}$, i.e.

$$\Omega_{\rm B}(\tau,\vec{x}) = \frac{1}{a^4(\tau)\rho_\gamma(\tau)} \frac{\vec{B}^2(\tau,\vec{x})}{8\pi}, \quad \partial_j \partial^i \tilde{\Pi}_j^i = (p_\gamma + \rho_\gamma) \nabla^2 \sigma_{\rm B} \tag{2.33}$$

where ρ_γ is the energy density of the photons. Since $\Omega_{\rm B}$ and $\sigma_{\rm B}$ are both quadratic in the magnetic field intensity, their corresponding two-point functions will be quartic in the magnetic field

intensities. Consequently $\Omega_{\rm B}$ and $\sigma_{\rm B}$ will have Fourier transforms that are defined as convolutions of the original magnetic fields and, more precisely:

$$\Omega_{\rm B}(\vec{x},\tau) = \frac{\delta\rho_{\rm B}(\vec{x},\tau)}{\rho_\gamma(\tau)} = \frac{1}{(2\pi)^{3/2}}\int d^3q\ \Omega_{\rm B}(\vec{q},\tau)e^{-i\vec{q}\cdot\vec{x}}, \quad \delta p_{\rm B} = \frac{\delta\rho_{\rm B}}{3}, \tag{2.34}$$

$$\sigma_{\rm B}(\vec{x},\tau) = \frac{1}{(2\pi)^{3/2}}\int d^3q e^{-i\vec{q}\cdot\vec{x}}\sigma_{\rm B}(\vec{q},\tau), \tag{2.35}$$

where

$$\Omega_{\rm B}(\vec{q},\tau) = \frac{1}{(2\pi)^{3/2}}\frac{1}{8\pi\bar{\rho}_\gamma}\int d^3p B_i(\vec{p})B^i(\vec{q}-\vec{p}), \tag{2.36}$$

$$\sigma_{\rm B}(\vec{q},\tau) = \frac{1}{(2\pi)^{3/2}}\frac{1}{16\pi\bar{\rho}_\gamma}\frac{1}{q^2}\int d^3p\Big[3(q^j-p^j)p^iB_j(\vec{p})B_i(\vec{q}-\vec{p}) - q^2B_i(\vec{q}-\vec{p})B^i(\vec{p})\Big]. \tag{2.37}$$

having defined, for notational convenience, $\bar{\rho}_\gamma = \rho_\gamma(\tau)a^4(\tau)$.

3 Large-scale solutions

After equality but before recombination the fluctuations of the geometry evolve coupled with the fluctuations of the plasma. The plasma contains four species: photons, neutrinos (that will be taken to be effectively massless at recombination), baryons and cold dark matter (CDM) particles. The evolution equations go under the name of Einstein-Boltzmann system since they are formed by the perturbed Einstein equations and by the evolution equations of the brightness perturbations. In the case of temperature autocorrelations, the relevant Boltzmann hierarchy will be the one associate with the *I* stokes parameter giving the intensity of the Thompson scattered radiation field. Furthermore, since neutrinos are collisionless after 1 MeV, the Boltzmann hierarchy for neutrinos has also to be consistently included. In practice, however, the lowest multipoles (i.e. the density contrast, the velocity and the anisotropic stress) will be the most important ones for the problem of setting the pre-recombination initial conditions.

Since stochastic magnetic fields are present prior to recombination, the Einstein-Boltzmann system has to be appropriately modified. This system has been already derived in the literature (see Ref. [34,35]) but since it will be heavily used in the present and in the following sections the main equations have been collected and discussed in appendix A. It is also appropriate to remark, on a more technical ground, that the treatment of the curvature perturbations demands the analysis of quantities that are invariant under infinitesimal coordinate transformations (or, for short,

gauge invariant). The strategy adopted in the appendix has been to pick up a specific gauge (i.e. the conformally Newtonian gauge) and to derive, in this gauge, the relevant evolution equations for the appropriate gauge-invariant quantities such as the density contrast on uniform density hypersurfaces (denoted, in what follows, by ζ) and the curvature perturbations on comoving orthogonal hypersurfaces (denoted, in what follows, by $\mathcal{R}$). Defining as k the comoving wavenumber of the fluctuations, the magnetized Einstein-Boltzmann system can be discussed in three complementary regimes:

• the wavelengths that are larger than the Hubble radius at recombination, i.e. $k\tau_{\rm rec} < 1$;

• the wavelengths that crossed the Hubble radius before recombination but that were still larger than the Hubble radius at equality, i.e. $k\tau_{\rm eq} < 1$;

• the wavelengths that crossed the Hubble radius prior to equality and that are, consequently, inside the Hubble radius already at equality (i.e. $k\tau_{\rm eq} > 1$).

The wavelengths that are larger than the Hubble radius at recombination determine the large-scale features of temperature autocorrelations and, in particular, the so-called Sachs-Wolfe plateau. The wavelengths that crossed the Hubble radius around $\tau_{\rm rec}$ determine the features of the temperature autocorrelations in the region of the Doppler oscillations.

The initial conditions of the Einstein-Boltzmann system are set in the regime when the relevant wavelengths are larger than the Hubble radius before equality (i.e. deep in the radiation epoch). The standard unknown is represented, in this context, by the primordial spectrum of the metric fluctuations whose amplitude and slope are two essential parameters of the ΛCDM model. To this unknown we shall also add the possible presence of a stochastically distributed magnetized background. In the conventional case, where magnetic fields are not contemplated, the system of metric fluctuations admits various (physically different) solutions that are customarily classified in adiabatic and non-adiabatic modes (see, for instance, [6,7] and also [13]). For the adiabatic modes the fluctuations of the specific entropy vanish at large scales. Conversely, for non-adiabatic (also sometimes named isocurvature) solutions the fluctuations of the specific entropy do not vanish. The WMAP 3-year data [1-3] suggest that the temperature autocorrelations are well fitted by assuming a primordial adiabatic mode of curvature perturbations with nearly scale-invariant power spectrum. Therefore, the idea will be now to assume the presence of an adiabatic mode of curvature perturbations and to scrutinize the effects of fully inhomogeneous magnetic fields. It should be again stressed that this is the minimal assumption compatible with the standard ΛCDM paradigm. As it will be briefly discussed later on, all the non-adiabatic solutions in the pre-equality regime can be generalized to include a magnetized background [35]. However, for making the discussion both more cogent and simpler, the attention will be focussed

on the physical system with the fewer number of extra-parameters, i.e. the case of a magnetized adiabatic mode.

3.1 Curvature perturbations

Consider the large angular scales that were outside the horizon at recombination. While smaller angular scales (compatible with the first Doppler peak) necessarily demand the inclusion of finite thickness effects of the last scattering surface, the largest angular scales (corresponding to harmonics $\ell \leq 25$) can be safely treated in the approximation that the visibility function is a Dirac delta function centered around $\tau_{\rm rec}$. Moreover, for the modes satisfying the condition $k\tau_{\rm rec} < 1$ the radiation-matter transition takes place when the relevant modes have wavelengths still larger than the Hubble radius.

It is practical, for the present purposes, to think the matter-radiation fluid as a unique physical entity with time-dependent barotropic index and time-dependent sound speed:

$$w_{\rm t}(\alpha) = \frac{p_{\rm t}}{\rho_{\rm t}} = \frac{1}{3(\alpha+1)}, \quad c_{\rm st}^2 = \frac{p_{\rm t}'}{\rho_{\rm t}'} = \frac{4}{3(4+3\alpha)}, \tag{3.1}$$

where $\alpha = a/a_{\rm eq}$. According to Eq. (3.1), when $a \gg a_{\rm eq}$ both $c_{\rm st}^2$ and $w_{\rm t}$ go to zero (as appropriate when matter dominates) while in the opposite limit (i.e. $\alpha << 1$) $c_{\rm st}^2 \simeq w_{\rm t} \to 1/3$ which is the usual result of the radiation epoch. Since recombination takes place after equality it will be crucial, for the present purposes, to determine the perturbations of the spatial curvature at this moment. The presence of fully inhomogeneous magnetic fields affects the evolution of the curvature perturbations across the radiation-matter transition. This issue has been addressed in [34] by following, outside the Hubble radius, the evolution of the gauge-invariant density contrast on uniform density hypersurfaces (customarily denoted by ζ):

$$\zeta = -\psi + \frac{\mathcal{H}(\delta\rho_{\rm t} + \delta\rho_{\rm B})}{\rho_{\rm t}'}. \tag{3.2}$$

where ψ is related to the fluctuation of the spatial component of the metric (i.e. $\delta_{\rm s} g_{ij} = 2a^2\psi\delta_{ij}$ in the conformally Newtonian gauge) and

$$\delta\rho_{\rm t} = \delta\rho_{\gamma} + \delta\rho_{\nu} + \delta\rho_{\rm c} + \delta\rho_{\rm b}, \quad \delta\rho_{\rm B} = \frac{B^2(\vec{x})}{8\pi a^4}, \tag{3.3}$$

are, respectively, the total density fluctuation of the fluid sources (i.e. photons, neutrinos, CDM and baryons) and the density fluctuations induced by a fully inhomogeneous magnetic field. The

gauge-invariant density contrast on uniform curvature hypersurfaces is related, via the Hamiltonian constraint (see Eq. (A.5)), to the curvature perturbations on comoving orthogonal hypersufaces customarily denoted by $\mathcal{R}$. Since both $\mathcal{R}$ and ζ are gauge-invariant, their mutual relation can be worked out in any gauge and, in particular, in the conformally Newtonian gauge where $\mathcal{R}$ can be expressed as [13]

$$\mathcal{R} = -\psi - \frac{2\rho_{\rm t}}{3(\rho_{\rm t}+p_{\rm t})}\left(\phi + \frac{\psi'}{\mathcal{H}}\right), \tag{3.4}$$

where ϕ is defined as the spatial part of the perturbed metric in the conformally Newtonian gauge, i.e. $\delta_{\rm s} g_{00} = 2a^2\phi$. In the same gauge the Hamiltonian constraint reads (see also appendix A and, in particular, Eq. (A.5))

$$\nabla^2\psi - 3\mathcal{H}(\mathcal{H}\phi + \psi') = 4\pi G a^2(\delta\rho_{\rm t} + \delta\rho_{\rm B}). \tag{3.5}$$

Using Eq. (2.5) inside Eq. (3.2) and inserting the obtained equation into Eq. (3.5) we obtain, through Eq. (3.4) the following relation

$$\zeta = \mathcal{R} + \frac{\nabla^2\psi}{12\pi G a^2(\rho_{\rm t}+p_{\rm t})}. \tag{3.6}$$

implying that [7] for $k\tau << 1$, $\mathcal{R}(k) \sim \zeta(k) + O(|k\tau|^2)$. From the covariant conservation equation we can easily deduce the evolution for ζ:

$$\zeta' = -\frac{\mathcal{H}}{p_{\rm t}+\rho_{\rm t}}\delta p_{\rm nad} + \frac{\mathcal{H}}{p_{\rm t}+\rho_{\rm t}}\left(c_{\rm st}^2 - \frac{1}{3}\right)\delta\rho_{\rm B} - \frac{\theta_{\rm t}}{3}. \tag{3.7}$$

In the case of a CDM-radiation entropy mode we have that

$$\delta p_{\rm nad} = \rho_{\rm M} c_{\rm s}^2 \mathcal{S}_*, \quad \mathcal{S}_* = \frac{\delta\zeta}{\zeta}, \tag{3.8}$$

where $\mathcal{S}_*$ is the relative fulctuation of the specific entropy $\zeta = T^3/n_{\rm CDM}$ defined in terms of the temperature T and in terms of the CDM concentration $n_{\rm CDM}$.

3.2 Magnetized adiabatic mode

The possible presence of entropic contributions will be neglected since the attention will now be focused on the simplest situation which implies solely the presence of an adiabatic mode. It is however useful to keep, for a moment, the dependence of the curvature perturbations also upon

$\mathcal{S}_*$ since the present analysis can be easily extended, with some algebra, to the case of magnetized non-adiabatic modes. Recalling now the expression of the total sound speed $c_{\rm st}^2$ given in Eq. (3.1) and noticing that

$$\frac{\rho_{\rm M}}{\rho_{\rm t}+p_{\rm t}}=\frac{3\alpha}{3\alpha+4}, \quad \frac{\rho_{\rm R}}{\rho_{\rm t}+p_{\rm t}}=\frac{3}{3\alpha+4}, \tag{3.9}$$

Eq. (3.7) can be recast in the following useful form [8]

$$\frac{d\zeta}{d\alpha}=-\frac{4\mathcal{S}_*}{(3\alpha+4)^2}-\frac{3R_\gamma\Omega_{\rm B}}{(3\alpha+4)^2}, \tag{3.10}$$

whose solution is

$$\zeta(k,\tau)=\zeta_*(k)-\frac{\alpha[4\mathcal{S}_*(k)+3R_\gamma\Omega_{\rm B}(k)]}{4(3\alpha+4)}, \tag{3.11}$$

where $\zeta_*(k)$ is the constant value of curvature perturbations implied by the presence of the adiabatic mode; $\Omega_{\rm B}(k)$ has been introduced in Eq. (2.36). The dependence upon the Fourier mode k has been explicitly written to remind that $\zeta_*(k)$ is constant in time but not in space. In the two relevant physical limits, i.e. well before and well after equality, Eq. (3.11) implies, respectively,

$$\lim_{\alpha\gg1}\zeta(k)=\zeta_*(k)-\frac{\mathcal{S}_*(k)}{3}-\frac{R_\gamma\Omega_{\rm B}(k)}{4}, \tag{3.12}$$

$$\lim_{\alpha\ll1}\zeta=\zeta_*(k)\frac{\mathcal{S}_*(k)}{4}\alpha-\frac{3R_\gamma\Omega_{\rm B}(k)}{16}\alpha. \tag{3.13}$$

When $\psi=\phi$ we can also obtain the evolution of ψ for the large scales

$$\frac{d\psi}{d\alpha}+\frac{5\alpha+6}{2\alpha(\alpha+1)}\psi=-\frac{3\alpha+4}{2\alpha(\alpha+1)}\zeta_*+\frac{4\mathcal{S}_*+3R_\gamma\Omega_{\rm B}}{8(\alpha+1)}. \tag{3.14}$$

Equation (3.14) can be easily solved by noticing that it can be rewritten as

$$\frac{\partial}{\partial\alpha}\left(\frac{\alpha^3}{\sqrt{\alpha+1}}\psi\right)\frac{\sqrt{\alpha+1}}{\alpha^3}=-\frac{3\alpha+4}{2\alpha(\alpha+1)}\zeta_*+\frac{4\mathcal{S}_*+3R_\gamma\Omega_{\rm B}}{8(\alpha+1)}, \tag{3.15}$$

implying that

$$\frac{\alpha^3}{\sqrt{\alpha+1}}\psi = -\frac{\zeta_*}{2}\mathcal{I}_1(\alpha) + \frac{4\mathcal{S}_*+3R_\gamma\Omega_{\rm B}}{8}\mathcal{I}_2(\alpha), \tag{3.16}$$

where

$$\mathcal{I}_1(\alpha)=\int_0^\alpha \frac{\beta^2(3\beta+4)}{(\beta+1)^{3/2}}d\beta, \quad \mathcal{I}_2(\alpha)=\int_0^\alpha \frac{\beta^3}{(\beta+1)^{3/2}}d\beta. \tag{3.17}$$

By using the obvious change of variables $\gamma = \beta + 1$ both integrals can be calculated with elementary methods with the result that

$$\begin{aligned}\mathcal{I}_1(\alpha) &= \frac{2\{16[\sqrt{\alpha+1}-1]+\alpha[\alpha(9\alpha+2)-8]\}}{15\sqrt{\alpha+1}},\\ \mathcal{I}_2(\alpha) &= \frac{2\{16[1-\sqrt{\alpha+1}]+\alpha[8+\alpha(\alpha-2)]\}}{5\sqrt{\alpha+1}}.\end{aligned} \tag{3.18}$$

Inserting Eq. (3.18) into Eq. (3.16) the explicit result for ψ can be written as:

$$\begin{aligned}\psi(k,\tau)=&-\frac{\zeta_*(k)}{15\alpha^3}\{16[\sqrt{\alpha+1}-1]+\alpha[\alpha(9\alpha+2)-8]\}\\ &+\frac{4\mathcal{S}_*(k)+3R_\gamma\Omega_{\rm B}(k)}{20\alpha^3}\{16[1-\sqrt{\alpha+1}]+\alpha[8+\alpha(\alpha-2)]\}.\end{aligned} \tag{3.19}$$

Equation (3.19) can be evaluated in the two limits mentioned above, i.e., respectively, well after and well before equality:

$$\begin{aligned}\lim_{\alpha\gg1}\psi(k,\tau)&=-\frac{3}{5}\zeta_*(k)+\frac{4\mathcal{S}_*(k)+3R_\gamma\Omega_{\rm B}(k)}{20},\\ \lim_{\alpha\ll1}\psi(k,\tau)&=-\frac{2}{3}\zeta_*(k)+\frac{\alpha}{32}\left[\frac{4}{3}\zeta_*(k)+4\mathcal{S}_*(k)+3R_\gamma\Omega_{\rm B}(k)\right].\end{aligned} \tag{3.20}$$

Notice that $\zeta_*(k)$ appears also in the correction which goes as $\alpha = a/a_{\rm eq}$. In this derivation the role of the anisotropic stress has been neglected. As full numerical solutions of the problem (in the tight coupling approximation) shows [35,36] that the magnetic anisotropic stress can be neglected close to recombination but it is certainly relevant deep in the radiation-dominated regime. To address this issue let us solve directly the system provided by the evolution equations of the longitudinal fluctuations of the geometry (i.e. Eqs. (A.4), (A.5) and (A.6)-(A.9))coupled with the evolution equations of the matter sources which are reported in appendix A. The evolution of the background will be the one dictated by Eq. (2.2) and by Eq. (2.6). The solution of the

Hamiltonian constraint (A.5) and of the evolution equations for various density contrasts (i.e. δ_ν, δ_γ, δ_b and δ_c) can be written, in the limit $x = \tau/\tau_1 << 1$ as

$$\begin{aligned}\delta_\gamma(k,\tau)&=\delta_\nu(k,\tau)=-2\phi_*(k)-R_\gamma\Omega_B(k)+4\psi_1(k)x,\\ \delta_c(k,\tau)&=\delta_c(k,\tau)=\frac{3}{4}\delta_\gamma(k,\tau).\end{aligned} \tag{3.21}$$

The Hamiltonian constraint (A.5) implies, always for $x << 1$, that the following relation must hold among the various constants:

$$\phi_1(k) + 3\psi_1(k) + \frac{\phi_*(k)}{2} = \frac{3}{4}R_\gamma\Omega_B(k). \tag{3.22}$$

Going on along the same theme we have that Eq. (A.9) is automatically satisfied by Eq. (3.21) in the small-x limit. The solution of Eq. (A.4) can be obtained with similar methods and always well before equality:

$$\sigma_\nu(k,\tau) = \frac{R_\gamma}{R_\nu}\sigma_B(k) + \frac{\kappa^2x^2}{6R_\nu}(\psi_*(k) - \phi_*(k)) + \frac{\kappa^2x^3}{6R_\nu}[(\psi_*(k) - \phi_*(k)) + (\psi_1(k) - \phi_1(k))], \tag{3.23}$$

where $\sigma_\nu(k, \tau)$ is the neutrino anisotropic stress and $\sigma_B(k, \tau)$ has been already introduced in Eq. (2.37); in Eq. (3.23) $\kappa = k\tau_1$ and it is the wave-number rescaled through τ_1 which appears in Eq. (2.2). Notice that, as $\Omega_B(k)$ also $\sigma_B(k)$ is approximately constant in time when the flux-freezing condition is verified. To derive Eq. (3.23) we take the $(i \neq j)$ component of the perturbed Einstein equation, i.e. Eq. (A.4) of the Appendix. From this equation we can write that:

$$\sigma_\nu = -\frac{R_\gamma}{R_\nu}\sigma_B + \frac{k^2}{6\mathcal{H}^2\Omega_R R_\nu}(\psi - \phi). \tag{3.24}$$

where, as usual, $x = \tau/\tau_1$ and where, according to Eqs. (2.2) and (2.6)

$$\begin{aligned}\mathcal{H}&=\frac{2(x+1)}{\tau_1 x(x+2)},\\ \Omega_R&=\frac{1}{(x+1)^2},\quad \Omega_M=\frac{x(x+2)}{(x+1)^2}.\end{aligned} \tag{3.25}$$

The solution for ψ and ϕ is parametrized as

$$\psi(k, \tau) = \psi_*(k) + \psi_1(k)x, \quad \phi(k, \tau) = \phi_* + \phi_1(k)x, \tag{3.26}$$

where the constants $\psi_*(k)$ and $\phi_1(k)$ will be determined by consistency with the other equations. Now we are interested in the solution valid for $x << 1$. So we have to expand all the terms of Eq. (3.24) for $x << 1$. Taking into account the exact form of $\mathcal{H}^2\Omega_R$, Eq. (3.24) becomes

$$\sigma_\nu = -\frac{R_\gamma}{R_\nu}\sigma_B + \frac{k^2\tau_1^2}{6R_\nu}x^2\left(1+\frac{x}{2}\right)^2[\psi-\phi). \tag{3.27}$$

Let us now expand the right hand side of Eq. (3.27). We will have that, for $x < 1$

$$\sigma_\nu = -\frac{R_\gamma}{R_\nu}\sigma_B + \frac{k^2\tau_1^2}{6R_\nu}x^2(1+x)[\psi_* - \phi_* + (\psi_1 - \phi_1)x]. \tag{3.28}$$

Rearranging the terms of Eq. (3.28) and keeping the terms $O(x^3)$, Eq. (3.23) can be immediately reproduced (recall, as previously posited, that $\kappa = k\tau_1$).

Using Eq. (3.21) into the evolution equations of the peculiar velocities (i.e. Eqs. (A.13), (A.18) and (A.25)), the explicit expressions for θ_c, θ_ν and $\theta_{\gamma b}$ can be easily obtained. In particular, for θ_c and θ_ν we have:

$$\theta_c(k,\tau) = \frac{\kappa^2}{2}\left[\phi_*(k)x+\frac{x^2}{6}(4\phi_1(k)-\phi_*(k))\right], \tag{3.29}$$

$$\theta_\nu(k,\tau) = \frac{\kappa^2 x}{4}\left[2\phi_*(k)+\frac{R_\gamma}{R_\nu}(4\sigma_B(k)-R_\nu\Omega_B(k))\right]+\frac{\kappa^2x^2}{2}[\psi_1(k)+\phi_1(k)]. \tag{3.30}$$

Finally, from Eq. (A.25), the photon-baryon peculiar velocity field is determined to be:

$$\theta_{\gamma b}(k,\tau) = \frac{\kappa^2 x}{8}[R_\nu\Omega_B(k) - 4\sigma_B(k) + 2\phi_*(k)] + \frac{\kappa^2x^2}{3}[\psi_1(k)+\phi_1(k)]. \tag{3.31}$$

By solving Eq. (A.19) (bearing in mind Eqs. (3.22) and (3.30)) the following relations can be obtained

$$\begin{aligned}
\psi_*(k) &= \left(1+\frac{2}{5}R_\nu\right)\phi_*(k)+\frac{R_\gamma}{5}[4\sigma_B(k)-R_\nu\Omega_B(k)],\\
\psi_1(k)-\phi_1(k) &= \frac{4}{15}R_\nu(\psi_1(k)+\phi_1(k))-\frac{2}{5}R_\nu\phi_*(k)-\frac{R_\gamma}{5}[4\sigma_B(k)-R_\nu\Omega_B(k)],
\end{aligned} \tag{3.32}$$

allowing to determine, in conjunction with Eq. (3.22), the explicit form of $\phi_1(k)$ and of $\psi_1(k)$:

$$\psi_1(k)=\frac{15+4R_\nu}{60+8R_\nu}\left[\frac{3}{4}R_\gamma\Omega_{\rm B}(k)-\frac{\phi_*(k)}{2}\right]-\frac{1}{60+8R_\nu}\left[\frac{2}{5}R_\nu\phi_*(k)+\frac{R_\gamma}{5}(4\sigma_{\rm B}(k)-R_\nu\Omega_{\rm B}(k))\right],$$
$$\phi_1(k)=\frac{15-4R_\nu}{60+8R_\nu}\left[\frac{3}{4}R_\gamma\Omega_{\rm B}(k)-\frac{\phi_*(k)}{2}\right]+\frac{3}{60+8R_\nu}\left[\frac{2}{5}R_\nu\phi_*(k)+\frac{R_\gamma}{5}(4\sigma_{\rm B}(k)-R_\nu\Omega_{\rm B}(k))\right]. \quad (3.33)$$

If $R_\nu = \Omega_{\rm B} = 0$ we have that

$$\phi_1(k) = \psi_1(k) = -\frac{\phi_*(k)}{8}, \quad (3.34)$$

and this result coincides precisely with the result already obtained in Eq. (3.13). In fact, recalling that $\alpha(x) = x^2 + 2x$, we have that, in the small-x region $\psi(k, \tau) \simeq -(2/3)\,\zeta_*(k) + (x/12)\,\zeta_*(k)$. But recalling now that, in the limit $R_\nu \to 0$ and $\Omega_{\rm B} \to 0$, $\zeta_*(k) = -(3/2)\psi_*(k)$, Eq. (3.34) is recovered. The obtained large-scale solutions will be important both for the explicit evaluation of the Sachs-Wolfe plateau as well as for the normalization of the solution at smaller k that will be discussed in the forthcoming section.

It is useful to add that, in the limit $(R_\gamma\sigma_{\rm B} + R_\nu\sigma_\nu) \to 0$ and $R_\nu \to 0$ the result reported in Eq.(3.11) is also recovered. Infact, in this limit, $\psi_* = \phi_*$ and $\zeta = \zeta_* + O(\alpha)$.

3.3 Estimate of the ordinary Sachs-Wolfe contribution

The ordinary and integrated Sachs-Wolfe contributions can now be computed. Recalling Eq. (A.45) the large-scale limit of the brightness perturbation of the radiation field is (see also Eqs. (A.40) and (A.45) of the appendix A)

$$\Delta_{\rm I}^{(\rm SW)}(\vec{k},\tau_0) = -\frac{\zeta_*(k)}{5} + \frac{R_\gamma\Omega_{\rm B}(k)}{20}, \quad (3.35)$$

$$\Delta_{\rm I}^{(\rm ISW)}(\vec{k},\tau_0) = \frac{10-4R_\nu}{5(15+4R_\nu)}\zeta_*(k) + \frac{3}{10}R_\gamma\Omega_{\rm B}(k) + \frac{4}{5}\frac{R_\gamma(R_\nu+5)(4\sigma_{\rm B}(k)-R_\nu\Omega_{\rm B}(k))}{5(15+4R_\nu)}. \quad (3.36)$$

As in the standard case, the ISW effect mimics the ordinary SW effect and it actually cancels partially the SW contribution at large angular scales. Notice that, in order to derive the explicit form of the ordinary SW it is practical to observe that, for wavelengths larger than the Hubble radius at recombination $(\delta_\gamma - 4\psi)' \simeq 0$. This observation implies that, clearly,

$\delta_{\gamma}^{(\mathrm{f})} = 4(\psi^{(\mathrm{f})} - \psi^{(\mathrm{i})}) + \delta_{\gamma}^{(\mathrm{i})}$ where the superscripts f (for final) and i (for initial) indicate that the values of the corresponding quantities are taken, respectively, well after and well before equality. The large angular scale expression of the temperature autocorrelations are defined as

$$C_{\ell}^{(\mathrm{SW})} = \frac{2}{\pi}\int k^3 d\ln k |\Delta_{\mathrm{I}}^{(\mathrm{SW})}(k,\tau_0)|^2. \tag{3.37}$$

To evaluate Eq. (3.37) in explicit terms we have to mention the conventions for the curvature and for the magnetic power spectra. The correlators of $\zeta_*(k)$, $\Omega_{\mathrm{B}}(k)$ and $\sigma_{\mathrm{B}}(k)$ are defined, respectively, as

$$\begin{aligned}
&\langle\zeta_*(\vec{k})\zeta_*(\vec{p})\rangle = |\zeta_*(k)|^2\delta^{(3)}(\vec{k}+\vec{p}),\\
&\langle\Omega_{\mathrm{B}}(\vec{k})\Omega_{\mathrm{B}}(\vec{p})\rangle = |\Omega_{\mathrm{B}}(k)|^2\delta^{(3)}(\vec{k}+\vec{p}),\\
&\langle\sigma_{\mathrm{B}}(\vec{k})\sigma_{\mathrm{B}}(\vec{p})\rangle = |\sigma_{\mathrm{B}}(k)|^2\delta^{(3)}(\vec{k}+\vec{p}).
\end{aligned} \tag{3.38}$$

In the case of the curvature perturbations we will have that

$$|\zeta_*(k)|^2 = \frac{2\pi^2}{k^3}\mathcal{P}_{\zeta}(k), \quad \mathcal{P}_{\zeta}(k) = \mathcal{A}_{\zeta}\left(\frac{k}{k_{\mathrm{p}}}\right)^{n_{\zeta}-1}, \tag{3.39}$$

where k_{p} denotes the pivot scale at which the spectrum of curvature fluctuations is computed and $\mathcal{A}_{\zeta}$ is, by definition, the amplitude of the spectrum at the pivot scale. In similar terms the magnetized contributions can be written as

$$|\Omega_{\mathrm{B}}(k)|^2 = \frac{2\pi^2}{k^3}\mathcal{P}_{\Omega}(k), \quad \mathcal{P}_{\Omega}(k) = \mathcal{F}(\varepsilon)\bar{\Omega}_{\mathrm{BL}}^2\left(\frac{k}{k_{\mathrm{L}}}\right)^{2\varepsilon}, \tag{3.40}$$

$$|\sigma_{\mathrm{B}}(k)|^2 = \frac{2\pi^2}{k^3}\mathcal{P}_{\sigma}(k), \quad \mathcal{P}_{\sigma}(k) = \mathcal{G}(\varepsilon)\bar{\Omega}_{\mathrm{BL}}^2\left(\frac{k}{k_{\mathrm{L}}}\right)^{2\varepsilon}, \tag{3.41}$$

where k_{L} (defined in Eq. (2.30)) denotes, in some sense, the magnetic pivot scale. The spectral index of the magnetic correlator defined in Eq. (2.32) is related to ε as $m + 3 = \varepsilon$. Notice also that in defining the correlators of Ω_{B} and of σ_{B} the same conventions used for the curvature perturbations have been adopted. These conventions imply that a factor k^{-3} appears at the right hand side of the first relation of Eq. (3.39).

Since the spectrum of the magnetic energy density implies the calculation of a convolution $\mathrm{k_L}$ is also related to the smoothing scale of the magnetic energy density (see, for instance, [35]). In

Eqs. (3.40) and (3.41) the functions $\mathcal{F}(\varepsilon)$ and $\mathcal{G}(\varepsilon)$ as well as the smoothed amplitude $\bar{\Omega}_{\rm BL}$ are defined as

$$\mathcal{F}(\varepsilon)=\frac{4(6-\varepsilon)(2\pi)^{2\varepsilon}}{\varepsilon(3-2\varepsilon)\Gamma^2(\varepsilon/2)}, \quad \mathcal{G}(\varepsilon)=\frac{4(188-4\varepsilon^2-66\varepsilon)(2\pi)^{2\varepsilon}}{3\varepsilon(3-\varepsilon)(2\varepsilon+1)\Gamma^2(\varepsilon/2)}, \tag{3.42}$$

$$\bar{\Omega}_{\rm BL}=\frac{\rho_{\rm BL}}{\bar{\rho}_\gamma}, \quad \rho_{\rm BL}=\frac{B_{\rm L}^2}{8\pi}, \quad \bar{\rho}_\gamma=a^4(\tau)\rho_\gamma(\tau). \tag{3.43}$$

From Eq. (3.43), recalling that $T_{\rm CMB}$ = 2.725K and that $\bar{\rho}_\gamma = (\pi^2/15)T_{\rm CMB}^4$, we can also write, in more explicit terms:

$$\bar{\Omega}_{\rm BL} = 7.565\times10^{-9}\left(\frac{B_{\rm L}}{\rm nG}\right)^2. \tag{3.44}$$

It should finally be appreciated that the power spectra of the magnetic energy density and of the anisotropic stress are proportional since we focus our attention to magnetic spectral slopes $\varepsilon < 1$ which are the most relevant at large length-scales [9]. In principle, the present analysis can be also extended to the case when the magnetic power spectra are very steep in k (i.e. $\varepsilon > 1$). In the latter case the power spectra are often said to be violet and they are severely constrained by thermal diffusivity effects [30].

By performing the integration over the comoving wave-number that appears in Eq. (3.37) the wanted result can be expressed as [10]

$$C_\ell^{\rm (SW)} = \left[\frac{\mathcal{A}_\zeta}{25}\mathcal{Z}_1(n_\zeta,\ell)+\frac{1}{400}R_\gamma^2\bar{\Omega}_{\rm BL}^2\mathcal{Z}_2(\varepsilon,\ell)-\frac{1}{50}\sqrt{\mathcal{A}_\zeta}R_\gamma\bar{\Omega}_{\rm BL}\mathcal{Z}_3(n_\zeta,\varepsilon,\ell)\cos\gamma_{br}\right], \tag{3.45}$$

where

$$\mathcal{Z}_1(n,\ell) = \frac{\pi^2}{4}\left(\frac{k_0}{k_{\rm P}}\right)^{n-1} 2^n \frac{\Gamma(3-n)\Gamma\left(\ell+\frac{n-1}{2}\right)}{\Gamma^2\left(2-\frac{n}{2}\right)\Gamma\left(\ell+\frac{5}{2}-\frac{n}{2}\right)}, \tag{3.46}$$

$$\mathcal{Z}_2(\varepsilon,\ell) = \frac{\pi^2}{2}\, 2^{2\varepsilon}\, \mathcal{F}(\varepsilon) \left(\frac{k_0}{k_L}\right)^{2\varepsilon} \frac{\Gamma(2-2\varepsilon)\Gamma(\ell+\varepsilon)}{\Gamma^2\left(\frac{3}{2}-\varepsilon\right)\Gamma(\ell+2-\varepsilon)}, \tag{3.47}$$

$$\mathcal{Z}_3(n,\varepsilon,\ell) = \frac{\pi^2}{4}\, 2^{\varepsilon}\, 2^{\frac{n+1}{2}} \sqrt{\mathcal{F}(\varepsilon)} \left(\frac{k_0}{k_L}\right)^{\varepsilon} \left(\frac{k_0}{k_{\rm p}}\right)^{\frac{n+1}{2}} \frac{\Gamma\left(\frac{5}{2}-\varepsilon-\frac{n}{2}\right)\Gamma\left(\ell+\frac{\varepsilon}{2}+\frac{n}{4}-\frac{1}{4}\right)}{\Gamma^2\left(\frac{7}{4}-\frac{\varepsilon}{2}-\frac{n}{4}\right)\Gamma\left(\frac{9}{4}+\ell-\frac{\varepsilon}{2}-\frac{n}{4}\right)}. \tag{3.48}$$

In Eq. (3.48) $\gamma_{\rm br}$ is the correlation angle that has been included to keep the expressions as general as possible. In what follows the main focus will however be on the case where the adiabatic mode of curvature perturbations is not correlated with the magnetized contribution (i.e. $\gamma_{\rm br} = \pi/2$). The various pivot scales appearing in Eqs. (3.46), (3.47) and (3.48) will now be defined:

$$k_{\rm p} = 0.002\ {\rm Mpc}^{-1}, \quad k_0 = \frac{h_0}{3000}\,{\rm Mpc}^{-1}, \quad k_{\rm L} = 1\ {\rm Mpc}^{-1}. \tag{3.49}$$

Let us now consider some simplified limits. The first one is to posit[11] $n_\zeta = 1$ and $\varepsilon < 1$. We will have that the functions $\mathcal{Z}$ will be simplified. They become:

$$\mathcal{Z}_1(1,\ell) = \frac{2\pi}{\ell(\ell+1)}, \tag{3.50}$$

$$\mathcal{Z}_2(\varepsilon,\ell) = \frac{\pi^2}{2}\, 2^{2\varepsilon}\, \mathcal{F}(\varepsilon) \left(\frac{k_0}{k_L}\right)^{2\varepsilon} \frac{\Gamma(2-2\varepsilon)\Gamma(\ell+\varepsilon)}{\Gamma^2\left(\frac{3}{2}-\varepsilon\right)\Gamma(\ell+2-\varepsilon)}, \tag{3.51}$$

$$\mathcal{Z}_3(1,\varepsilon,\ell) = \frac{\pi^2}{2}\, 2^{\varepsilon} \sqrt{\mathcal{F}(\varepsilon)} \left(\frac{k_0}{k_L}\right)^{\varepsilon} \left(\frac{k_0}{k_{\rm p}}\right) \frac{\Gamma(2-\varepsilon)\Gamma\left(\ell+\frac{\varepsilon}{2}\right)}{\Gamma^2\left(\frac{3}{2}-\frac{\varepsilon}{2}\right)\Gamma\left(\ell+2-\frac{\varepsilon}{2}\right)}. \tag{3.52}$$

We now can enforce the normalization at large scales by assuming a dominant adiabatic mode. A preliminary manipulation is the following. We can write the previous expression as

$$\frac{\ell(\ell+1)}{2\pi} C_\ell^{\rm (SW)} = \frac{\mathcal{A}_\zeta}{25}\left[1 + \left(\frac{R_\gamma^2}{16\mathcal{A}_\zeta}\bar{\Omega}_{\rm BL}^2\right)\frac{\ell(\ell+1)}{2\pi}\mathcal{Z}_2(\varepsilon,\ell) - \left(\frac{R_\gamma}{2\sqrt{\mathcal{A}_\zeta}}\bar{\Omega}_{\rm BL}\right)\frac{\ell(\ell+1)}{2\pi}\mathcal{Z}_3(1,\varepsilon,\ell)\cos\gamma_{\rm br}\right]. \tag{3.53}$$

We can now expand the relevant terms in powers of ε. We do get

$$\frac{\ell(\ell+1)}{2\pi}C_{\ell}^{(\mathrm{SW})}=\frac{\mathcal{A}_{\zeta}}{25}\left[1+Q_1(\ell)\left(\frac{R_{\gamma}^2}{16\mathcal{A}_{\zeta}}\bar{\Omega}_{\mathrm{BL}}^2\right)\mathcal{F}(\varepsilon)\left(\frac{k_0}{k_{\mathrm{L}}}\right)^{2\varepsilon}-Q_2(\ell)\left(\frac{R_{\gamma}}{2\sqrt{\mathcal{A}_{\zeta}}}\bar{\Omega}_{\mathrm{BL}}\right)\sqrt{\mathcal{F}(\varepsilon)}\left(\frac{k_0}{k_{\mathrm{L}}}\right)^{\varepsilon}\left(\frac{k_0}{k_{\mathrm{p}}}\right)\right], \tag{3.54}$$

where

$$\begin{aligned} Q_1(\ell)&=1+\left(2+\frac{1}{\ell}+\frac{1}{\ell+1}-2\ln 2+2\frac{\Gamma'(\ell)}{\Gamma(\ell)}\right)\varepsilon+O(\varepsilon^2),\\ Q_2(\ell)&=\frac{1}{2}Q_1(\ell). \end{aligned} \tag{3.55}$$

We can then compute the various pieces. They will set the scale of the numerical results. In particular, it is easy to argue that the presence of the cross correlation enhances the results at smaller scales. As a final comment it is relevant to remark that the large-scale solutions are not only important per se but they will be used to deduce the appropriate normalization for the results arising at smaller angular scales.

4 Intermediate scales

As discussed in the previous section the attention will now be focussed on the situation of a dominant adiabatic mode. This is just because we want to delicately extend the ΛCDM paradigm and make contact with the standard scenario. In fact, it should be clear that our attempts are not alternative to the standard lore but, more modestly, complementary.

From Eqs. (A.32), (A.33) and (A.34) the photon density contrast can be determined under the assumption that the entropic contribution is absent. Thus, if only the magnetic fields and the adiabatic mode are present, Eqs. (A.34), (A.35) and (A.36) lead to the following solution

$$\delta_{\gamma}(k,\tau)=-\frac{4}{3c_{\mathrm{sb}}^2}\psi(k,\tau)+[4\sigma_{\mathrm{B}}(k)-\Omega_{\mathrm{B}}(k)]+\sqrt{c_{\mathrm{sb}}}A_1(k)\cos[\alpha(\tau,k)]e^{-\frac{k^2}{k_{\mathrm{D}}^2}}, \tag{4.1}$$

where $\psi(k, \tau)$ is assumed to be slowly varying in time and where, recalling Eq. (2.8)

$$\alpha(\tau,k)=k\int_0^{\tau_{\mathrm{rec}}}c_{\mathrm{sb}}(\tau)d\tau, \quad \frac{1}{k_{\mathrm{D}}^2}=\frac{2}{5}\int\lambda_{\mathrm{T}}(\tau)c_{\mathrm{sb}}^2(\tau)d\tau. \tag{4.2}$$

The constant $A_1(k)$ can be determined by matching the solution to the large-scale (i.e. super-Hubble) behaviour of the fluctuations, i.e.

$$\frac{\delta_\gamma(k,\tau)}{4}+\psi(k,\tau)\to\frac{\psi_{\rm m}(k)}{3}=-\frac{\zeta_*(k)}{5}+\frac{R_\gamma}{20}\Omega_{\rm B}(k), \tag{4.3}$$

where $\psi_{\rm m}$ denotes the value of $\psi(k)$ after equality and for $k\tau < 1$. From the solution of the evolution equation of $\delta_\gamma(k,\ \tau)$ also $\theta_{\gamma{\rm b}}(k,\ \tau)$ can be easily obtained (see, in particular, Eq. (A.24) of appendix A). The final result can be expressed, for the present purposes, as[12]

$$\left[\frac{\delta_\gamma(k,\tau)}{4}+\psi(k,\tau)\right]=\mathcal{L}_\zeta(k,\tau)+[\mathcal{M}_\zeta(k,\tau)\mathcal{D}_\zeta(k)+\mathcal{M}_{\rm B}(k,\tau)\mathcal{D}_{\rm B}(k)]\sqrt{c_{\rm sb}}\cos[\alpha(\tau,k)], \tag{4.4}$$

$$\theta_{\gamma{\rm b}}(k,\tau)=3c_{\rm sb}^{3/2}[\mathcal{M}_\zeta(k,\tau)\mathcal{D}_\zeta(k)+\mathcal{M}_{\rm B}(k,\tau)\mathcal{D}_{\rm B}(k)]\sin[\alpha(\tau,k)]. \tag{4.5}$$

The functions $\mathcal{L}_\zeta(k,\ \tau)$ and $\mathcal{M}_\zeta(k,\ \tau)$ are directly related to the curvature perturbations and can be determined by interpolating the large-scale behaviour with the small-scale solutions. In the present case they can be written as

$$\mathcal{L}_\zeta(k,\tau)=-\frac{\zeta_*(k)}{6}\left(1-\frac{1}{3c_{\rm sb}^2}\right)\ln\left[\frac{14}{w\ell}\frac{\tau_0}{\tau_{\rm eq}}\right], \tag{4.6}$$

$$\mathcal{M}_\zeta(k,\tau)=-\frac{6}{25}\zeta_*(k)\ln\left[\frac{14}{25}w\ell\frac{\tau_{\rm eq}}{\tau_0}\right]. \tag{4.7}$$

In Eqs. (4.6) and (4.7) the variable $w = k\tau_0/\ell$ has been introduced. This way of writing may seem, at the moment, obscure. However, the variable w will appear as integration variable in the angular power spectrum, so it is practical, as early as possible, to express the integrands directly in terms of w. Finally the functions $\mathcal{L}_{\rm B}(k,\ \tau)$ and $\mathcal{M}_{\rm B}(k,\ \tau)$ are determined in similar terms and they can be written as

$$\mathcal{L}_{\rm B}(k,\tau)=\frac{3R_\gamma}{20}\Omega_{\rm B}(k)\left(1-\frac{1}{3c_{\rm sb}^2}\right)+\left[\sigma_{\rm B}(k)-\frac{\Omega_{\rm B}(k)}{4}\right], \tag{4.8}$$

$$\mathcal{M}_{\rm B}(k,\tau)=3^{1/4}\left\{\left[\frac{\Omega_{\rm B}}{4}(k)-\sigma_{\rm B}(k)\right]+\frac{R_\gamma}{20}\Omega_{\rm B}(k)\right\}. \tag{4.9}$$

It should be stressed that Eqs. (4.6) and (4.7) can be obtained from the standard form of the ΛCDM transfer function in the case when $\Omega_{b0} << \Omega_{M0}$ and for a spatially flat Universe. Under these assumptions (which are the ones clearly spelled out at the beginning of the present paper) the transfer function (conventionally denoted by $T(q)$) will depend solely upon $q = k/(14k_{eq})$. When $k_{eq} < k < 11k_{eq}$(which is the interesting range if we want to study the first two Doppler peaks), then the full transfer function $T(q)$ given in [57] can be approximated by $T(k) \simeq (1/4) \ln [14k_{eq}/k]$, which leads to Eq. (4.6) once we recall the definition of w and once we normalize, at large-scales, the SW contribution to the adiabatic initial conditions in the presence of the magnetized contribution derived before in the long wavelength limit.

The functions $\mathcal{D}_{\zeta}(k)$ and $\mathcal{D}_{B}(k)$ encode the informations related to the diffusivity wavenumber:

$$\mathcal{D}_{\zeta}(k) = e^{-\frac{k^2}{k_D^2}}, \quad \mathcal{D}_{B}(k) = e^{-\frac{k^2}{k_B^2}}. \tag{4.10}$$

As introduced before k_D is the thermal diffusivity scale (i.e. shear viscosity). The quantity named k_B is the smallest momentum between the ones defined by magnetic diffusivity, by Alfvén diffusivity and by thermal diffusivity. The magnetic diffusivity has been already introduced in Eq. (2.21) and it arises because of the finite value of the conductivity. The Alfvén diffusivity arises when the magnetic field supports Alfvén waves that are subsequently damped for typical length-scales that are a bit smaller than the Silk damping scale (see [30] and, in particular, [55]). Now, if the magnetic field is fully inhomogeneous (as in the present case) the dominant source of diffusivity is represented by the Silk length scale since it is larger than the magnetic diffusivity length and than the Alfvén diffusivity length [30]. For the purpose of simplifying the integrals to be evaluated numerically it is practical to introduce the following rescaled quantities:

$$\begin{aligned} \mathcal{L}_{\zeta}(k,\tau) &= \zeta_{*}(k) L_{\zeta}(k,\tau), \qquad \mathcal{L}_{B}(k,\tau) = \Omega_{B}(k) L_{B}(k,\tau), \\ \mathcal{M}_{\zeta}(k,\tau) &= \zeta_{*}(k) M_{\zeta}(k,\tau), \quad \mathcal{M}_{B}(k,\tau) = \Omega_{B}(k) M_{B}(k,\tau), \end{aligned} \tag{4.11}$$

after some algebra the angular power spectrum can be written as the sum of four integrals, i.e.

$$C_{\ell} = \mathcal{U}_1(\ell) + \mathcal{U}_2(\ell) + \mathcal{U}_3(\ell) + \mathcal{U}_4(\ell), \tag{4.12}$$

where:

$$\mathcal{U}_1(\ell) = 4\pi \int_0^{\infty} \frac{dw}{w} \bar{\mathcal{U}}_1(\ell,w) \mathcal{K}^2(\ell,\ell_t,w) j_{\ell}^2(\ell w), \tag{4.13}$$

$$\mathcal{U}_2(\ell) = 2\pi c_{\rm sb}\int_0^\infty \frac{dw}{w^3}[w^2+9c_{\rm sb}^2(w^2-1)]\bar{\mathcal{U}}_2(\ell,w)\mathcal{K}^2(\ell,\ell_{\rm t},w)j_\ell^2(\ell w), \tag{4.14}$$

$$\mathcal{U}_3(\ell) = 2\pi c_{\rm sb}\int_0^\infty \frac{dw}{w^3}[w^2-9c_{\rm sb}^2(w^2-1)]\bar{\mathcal{U}}_3(\ell,w)\cos(2\ell\gamma w)\mathcal{K}^2(\ell,\ell_{\rm t},w)j_\ell^2(\ell w), \tag{4.15}$$

$$\mathcal{U}_4(\ell) = 8\pi\sqrt{c_{\rm sb}}\int_0^\infty \frac{dw}{w}\cos(\ell\gamma w)\bar{\mathcal{U}}_4(\ell,w)\mathcal{K}^2(\ell,\ell_{\rm t},w)j_\ell^2(\ell w), \tag{4.16}$$

where $j\ell(\gamma)$ denote the spherical Bessel functions of the first kind [52,53] which are related to the ordinary Bessel functions of the first kind as $j_{\ell=\sqrt{\pi/(2\gamma)}J_{\ell+1/2}(\gamma)}$. The various functions appearing in Eqs. (4.13), (4.14), (4.15) and (4.16) are:

$$\begin{aligned}\bar{\mathcal{U}}_1(\ell,w) &= \mathcal{P}_\zeta(w,\ell)L_\zeta^2(\ell,w)+\mathcal{P}_\Omega(w,\ell)L_{\rm B}^2(\ell,w)\\ &+ 2L_\zeta(\ell,w)L_{\rm B}(\ell,w)\sqrt{\mathcal{P}_\zeta(w,\ell)}\sqrt{\mathcal{P}_\Omega(w,\ell)},\end{aligned} \tag{4.17}$$

$$\begin{aligned}\bar{\mathcal{U}}_2(\ell,w) &= \mathcal{P}_\zeta(w,\ell)M_\zeta^2(\ell,w)\mathcal{D}_\zeta^2(\ell,\ell_{\rm S},w)+\mathcal{P}_\Omega(w)M_{\rm B}^2(\ell,w)\mathcal{D}_B^2(\ell,\ell_{\rm A},w)\\ &+ 2\sqrt{\mathcal{P}_\zeta(w,\ell)}\sqrt{\mathcal{P}_\Omega(w,\ell)}M_\zeta(\ell,w)M_{\rm B}(\ell,w)\mathcal{D}_\zeta(\ell,\ell_{\rm S},w)\mathcal{D}_{\rm B}(\ell,\ell_{\rm A},w),\end{aligned} \tag{4.18}$$

$$\begin{aligned}\bar{\mathcal{U}}_3(\ell,w) &= \mathcal{P}_\zeta(w,\ell)M_\zeta^2(\ell,w)\mathcal{D}_\zeta^2(\ell,\ell_{\rm t},w)+\mathcal{P}_\Omega(w,\ell)(\ell,\ell_{\rm A},w)M_{\rm B}^2(\ell,w)\mathcal{D}_B^2\\ &+ 2\sqrt{\mathcal{P}_\zeta(w,\ell)}\sqrt{\mathcal{P}_\Omega(w,\ell)}M_\zeta(\ell,w)M_{\rm B}(\ell,w)\mathcal{D}_\zeta(\ell,\ell_{\rm S},w)\mathcal{D}_{\rm B}(\ell,\ell_{\rm A},w),\end{aligned} \tag{4.19}$$

$$\begin{aligned}\bar{\mathcal{U}}_4(\ell,w) &= \mathcal{P}_\zeta(w,\ell)L_\zeta(\ell,w)M_\zeta(\ell,w)\mathcal{D}_\zeta(\ell,\ell_{\rm S},w)+\mathcal{P}_\Omega(w,\ell)L_{\rm B}(\ell,w)M_{\rm B}(\ell,w)\mathcal{D}_{\rm B}(\ell,\ell_{\rm A},w)\\ &+ \sqrt{\mathcal{P}_\zeta(w,\ell)}\sqrt{\mathcal{P}_\Omega(w,\ell)}L_\zeta(\ell,w)M_{\rm B}(\ell,w)\mathcal{D}_{\rm B}(\ell,\ell_{\rm A},w)\\ &+ \sqrt{\mathcal{P}_\zeta(w,\ell)}\sqrt{\mathcal{P}_\Omega(w,\ell)}L_{\rm B}(\ell,w)M_\zeta(\ell,w)\mathcal{D}_\zeta(\ell,\ell_{\rm S},w),\end{aligned} \tag{4.20}$$

where $\ell_{\rm S}$ and $\ell_{\rm A}$ denote respectively the typical Silk multipole and the typical multipole associated with Alfvén diffusivity. They will be defined explicitly in a moment. In Eqs. (4.15) and (4.16) the oscillatory terms arising, originally, in the full expression of the angular power spectrum have been simplified. The two oscillatory contributions in Eqs. (4.15) and (4.16) go, respectively, as cos ($2\gamma\ell w$) and as cos ($\gamma\ell w$). The definition of γ can be easily deduced from the original parametrization of the oscillatory contribution in Eqs. (4.1) and (4.2). In fact we can write $\alpha(k,$

$\tau_{\rm rec}) = \gamma(\tau_{\rm rec})\,\ell w$. Recalling that $w = k\tau_0/\ell$, and defining, for notational convenience, $\gamma \equiv \gamma(\tau_{\rm rec})$, the following expression for γ can be easily obtained

$$\gamma = \frac{1}{\tau_0}\int_0^{\tau_{\rm rec}} c_{\rm sb}(\tau)d\tau = \frac{\tau_1}{\sqrt{3}\tau_0}\int_0^{\tau_{\rm rec}/\tau_1}\frac{dx}{\sqrt{1+\nu_1(x^2+2x)}}. \tag{4.21}$$

In Eq. (4.21) the first equality is simply the definition of γ while the second equality can be deduced by inserting in the definition the explicit expression of the scale factor of Eq. (2.2). By doing so the constant ν_1 is just $R_{\rm b}z_{\rm rec}/z_{\rm eq}$. The expression of γ can be made even more explicit by performing the integral appearing in Eq. (4.21):

$$\gamma = \frac{1}{\sqrt{3}}\left(\frac{\tau_1}{\tau_0}\right)\sqrt{\frac{z_{\rm eq}}{z_{\rm rec}}}\,\ln\left[\frac{\nu_1(1+x_{\rm rec})+\sqrt{1+\nu_1 x_{\rm rec}(x_{\rm rec}+2)}}{\sqrt{\nu_1}+1}\right], \quad x_{\rm rec} = \frac{\tau_{\rm rec}}{\tau_1}. \tag{4.22}$$

It is now practical to recall that the ratio between τ_1 and τ_0 depends upon the critical fraction of the dark energy. So the scale factor (2.2) must be complemented, at late times, by the contribution of the dark energy. This standard calculation leads to the following estimate for a spatially flat Universe

$$\frac{\tau_1}{\tau_0} = \frac{\tau_1}{\tau_{\rm rec}}\frac{\tau_{\rm rec}}{\tau_0} = \frac{\mathcal{I}_\Lambda}{\sqrt{z_{\rm eq}}}, \quad \mathcal{I}_\Lambda = |1-\Omega_{\Lambda 0}|^{-\nu_2}, \tag{4.23}$$

where $\Omega_{\Lambda 0}$ is the present critical fraction of dark energy (parametrized in terms of a cosmological constant in a ΛCDM framework) and where $\nu_2 = 0.0858$. Inserting Eq. (2.9) into Eq. (4.23) and recalling the explicit expression of ν_1 we will have finally

$$\gamma = \frac{\mathcal{I}_\Lambda}{\sqrt{3R_{\rm b}z_{\rm rec}}}\ln\left[\frac{\sqrt{(1+z_{\rm rec}/z_{\rm eq})R_{\rm b}}+\sqrt{1+R_{\rm b}}}{1+\sqrt{R_{\rm b}z_{\rm rec}/z_{\rm eq}}}\right]. \tag{4.24}$$

At this point the spherical Bessel functions appearing in the above expressions can be evaluated in the limit of large ℓ with the result that the above expressions can be made more explicit. In particular, focussing the attention on $j\ell(\ell w)$, we have that [52,53]

$$j_\ell^2(\ell w) \simeq \frac{\cos^2[\beta(w,\ell)]}{\ell w\sqrt{\ell^2 w^2 - \ell^2}}, \quad w > 1. \tag{4.25}$$

Note that the expansion (4.25) has been used consistently by other authors (see, in particular, [44,45] and also [39,41-43]). The result expressed by Eq. (4.25) allows to write the integrals of Eqs. (4.13), (4.14), (4.15) and (4.16) as

$$C_\ell = \frac{1}{\ell^2}[C_1(\ell)+C_2(\ell)+C_3(\ell)+C_4(\ell)], \tag{4.26}$$

where

$$C_1(\ell) = \int_1^\infty I_1(w,\ell)\bar{\mathcal{U}}_1(\ell,w)dw, \tag{4.27}$$

$$C_2(\ell) = \int_1^\infty I_2(w,\ell)\bar{\mathcal{U}}_2(\ell,w)dw, \tag{4.28}$$

$$C_3(\ell) = \int_1^\infty I_3(w,\ell)\bar{\mathcal{U}}_3(\ell,w)dw, \tag{4.29}$$

$$C_4(\ell) = \int_1^\infty I_4(w,\ell)\bar{\mathcal{U}}_4(\ell,w)dw, \tag{4.30}$$

where

$$I_1(w,\ell) = \frac{4\pi\cos^2[\beta(w,\ell)]}{w^2\sqrt{w^2-1}} e^{-2\frac{\ell^2}{\ell_t^2}w^2}, \tag{4.31}$$

$$I_2(w,\ell) = 2\pi c_{sb}\frac{w^2+9c_{sb}^2(w^2-1)}{w^4\sqrt{w^2-1}}\cos^2[\beta(w,\ell)]e^{-2\frac{\ell^2}{\ell_t^2}w^2}, \tag{4.32}$$

$$I_3(w,\ell) = 2\pi c_s\frac{w^2+9c_{sb}^2(w^2-1)}{w^4\sqrt{w^2-1}}\cos(2\ell\gamma w)\cos^2[\beta(w,\ell)]e^{-2\frac{\ell^2}{\ell_t^2}w^2}, \tag{4.33}$$

$$I_4(w,\ell) = 8\pi\sqrt{c_{sb}}\frac{\cos(\ell\gamma w)}{w^2\sqrt{w^2-1}}\cos^2[\beta(w,\ell)]e^{-2\frac{\ell^2}{\ell_t^2}w^2}. \tag{4.34}$$

Concerning Eqs. (4.27)–(4.30) and (4.31)–(4.34) the following comments are in order:

• the lower limit of integration over w is 1 in Eqs. (4.27)–(4.30) since the asymptotic expansion of Bessel functions implies that $k_{\tau 0} \geq \ell$, i.e. $w \geq 1$;

• the obtained expressions will be valid for the angular power spectrum will be applicable for sufficiently large ℓ; in practice, as we shall see the obtained results are in good agreement with the data in the Doppler region;

• the function $\beta(w,\ell)=\ell\sqrt{w^2-1}-\ell\ \arccos\ (w^{-1})-\frac{\pi}{4}$ leads to a rapidly oscillating argument whose effect will be to slow down the convergence of the numerical integration; it is practical, for the present purposes, to replace $\cos^2[\beta(w,\ell)]$ by its average (i.e. 1/2).

In the integrals (4.31), (4.32), (4.33) and (4.34) the scale $\ell_{\rm t}$ stems from the finite thickness of the last scattering surface and it is defined as

$$\ell_{\rm t}^2=\frac{1}{4\sigma^2}\left(\frac{\tau_0}{\tau_{\rm rec}}\right)^2,\quad \sigma=1.49\times10^{-2}\,\frac{\sqrt{z_{\rm rec}+z_{\rm eq}}+\sqrt{z_{\rm rec}}}{\sqrt{z_{\rm rec}+z_{\rm eq}}}. \tag{4.35}$$

Furthermore, within the present approximations,

$$\frac{\ell_{\rm t}^2}{\ell_{\rm S}^2}=\frac{\sigma^2k_{\rm D}^2\tau_{\rm rec}^2}{\sigma^2k_{\rm D}^2\tau_{\rm rec}^2+1},\quad \ell_{\rm A}\simeq\ell_{\rm S} \tag{4.36}$$

To simplify further the obtained expressions we can also change variable in some of the integrals. Consider, as an example, the integrals appearing in the expression of $C_1(\ell)$ (see Eq. (4.27)). Changing the variable of integration as $w = \gamma^2 + 1$ we will have that

$$C_1(\ell)=\int_0^\infty \bar{I}_1(\gamma,\ell)\bar{\mathcal{U}}_1(\ell,\gamma)d\gamma, \tag{4.37}$$

where, in explicit terms and after the change of variables,

$$\bar{I}_1(\gamma,\ell)=\frac{4\pi}{(\gamma^2+1)^2\sqrt{\gamma^2+2}}e^{-2\frac{\ell^2}{\ell_{\rm t}^2}(\gamma^2+1)^2}, \tag{4.38}$$

and

$$\begin{aligned}\bar{\mathcal{U}}_1(\ell,\gamma) &= \mathcal{A}_\zeta\left(\frac{k_0}{k_{\rm p}}\right)^{n-1}\ell^{n-1}L_\zeta^2(\ell,\gamma)(\gamma^2+1)^{n-1}+\bar{\Omega}_{\rm BL}^2\left(\frac{k_0}{k_{\rm L}}\right)^{2\varepsilon}\ell^{2\varepsilon}\mathcal{F}(\varepsilon)L_{\rm B}^2(\ell,\gamma)(\gamma^2+1)^{2\varepsilon}\\ &+ 2L_{\rm B}(\ell,\gamma)L_\zeta(\ell,\gamma)\sqrt{\mathcal{A}_\zeta}\bar{\Omega}_{\rm BL}\ell^{(n-1)/2+\varepsilon}\sqrt{\mathcal{F}(\varepsilon)}\left(\frac{k_0}{k_{\rm p}}\right)^{(n-1)/2}\left(\frac{k_0}{k_{\rm L}}\right)^{\varepsilon}(\gamma^2+1)^{(n-1)/2+\varepsilon}.\end{aligned} \tag{4.39}$$

In Eq. (4.39) the explicit dependence of the functions $L_{\mathrm{B}}(\ell, \gamma)$ and $L_{\zeta}(\ell, \gamma)$ upon γ can be simply deduced from the analog expressions in terms of w :

$$L_{\zeta}(\ell,\gamma) = -\frac{1}{6}\left(1-\frac{1}{3c_{\mathrm{sb}}^{2}}\right)\ln\left[\frac{14}{\ell(\gamma^{2}+1)}\frac{\tau_{0}}{\tau_{\mathrm{eq}}}\right],$$
$$L_{\mathrm{B}}(\ell,\gamma) = \frac{3R_{\gamma}}{20}\left(1-\frac{1}{3c_{\mathrm{sb}}^{2}}\right)+\left[\frac{\mathcal{G}(\varepsilon)}{\mathcal{F}(\varepsilon)}-\frac{1}{4}\right]. \tag{4.40}$$

With similar manipulations it is possible to transform also all the other integrands appearing in Eqs. (4.28), (4.29) and (4.30).

5 Calculation of the temperature autocorrelations

So far the necessary ingredients for the estimate of the magnetized temperature autocorrelations have been sorted out. In particular the angular power spectrum has been computed semi-analytically in the two relevant regions, i.e. the Sachs-Wolfe regime (corresponding to large angular scales and $\ell \leq 30$) and the Doppler region, i.e. $\ell > 100$. Furthermore, for the nature of the approximations made we do not expect the greatest accuracy of the algorithm in the intermediate region (i.e. $30 < \ell < 100$). Indeed, it was recognized already in the absence of magnetic fields that it is somehow necessary to smooth the joining of the two regimes by assuming an interpolating form of the metric fluctuations that depends upon two fitting parameters [42,43]. We prefer here to stress that this method is inaccurate in the matching regime since the spherical Bessel functions have been approximated for large ℓ. Therefore, the comparison with experimental data should be preferentially conducted, for the present purposes, in the Doppler region. The strategy adopted in the present section is, therefore, the following:

• by taking a concordance model as a starting point, the shape and amplitude of the Doppler oscillations will be analyzed when the amplitude and spectral slope of the stochastic field are allowed to vary;

• constraints can then be derived from the temperature autocorrelations induced by the simultaneous presence of the standard adiabatic mode and of the stochastic magnetic field.

Before plunging into the discussion, it is appropriate to comment on the choice of the cosmological parameters that will be employed throughout this section. The WMAP 3-year [1] data have been combined, so far, with various sets of data. These data sets include the 2dF Galaxy Redshift Survey [58], the combination of Boomerang and ACBAR data [59,60], the combination of CBI and VSA data [61,62]. Furthermore the WMAP 3-year data can be also combined with the Hubble Space Telescope Key Project (HSTKP) data [63] as well as with the Sloan Digital Sky Survey

(SDSS) [64,65] data. Finally, the WMAP 3-year data can be also usefully combined with the weak lensing data [66,67] and with the observations of type Ia supernovae [13](SNIa). Each of the data sets mentioned in the previous paragraph can be analyzed within different frameworks. The minimal ΛCDM model with no cut-off in the primordial spectrum of the adiabatic mode and with vanishing contribution of tensor modes is the simplest concordance framework. This is the one that has been adopted in this paper. Diverse completions of this minimal model are possible: they include the addition of the tensor modes, a sharp cut-off in the spectrum and so on and so forth. One of the conclusions of the present study is that the observational cosmologists may also want to include, in their analyses, the possibility of pre-recombination large-scale magnetic fields.

All these sets of data (combined with different theoretical models) lead necessarily to slightly different determinations of the relevant cosmological parameters To have an idea of the range of variations of the parameters the following examples are useful[14]:

• the WMAP 3-year data alone [1] (in a ΛCDM framework) seem to favour a slightly smaller value $h_0^2\Omega_{\mathrm{M0}} = 0.127$;

• if the WMAP 3-year data are combined with the "gold" sample of SNIa [69] (see also [70]) the favoured value is $h_0^2\Omega_{\mathrm{M0}}$ is of the order of 0.134; if the WMAP 3-year data are combined with *all* the data sets $h_0^2\Omega_{\mathrm{M0}} = 0.1324$.

• similarly, if the WMAP data alone are considered, the preferred value of $h_0^2\Omega_{\mathrm{b0}}$ is 0.02229 while this value decreases to 0.02186 if the WMAP data are combined with all the other data sets.

The aforementioned list of statements refers to the case of a pure ΛCDM model. If, for instance, tensors are included, then the WMAP 3-year data combined with CBI and VSA increase a bit the value of $h_0^2\Omega_{\mathrm{b0}}$ which becomes, in this case closer to 0.023. While in the future it might be interesting to include pre-recombination magnetic fields also in non-minimal ΛCDM scenarios, here the logic will be to take a best fit model to the WMAP data alone, compare it with the numerical scheme proposed in this paper, and, consequently, assess the accuracy of the semi-analytical method. Once this step will be concluded the effects stemming from the presence of the magnetic fields will be carefully analyzed. Consider, therefore, the case when the magnetic field vanishes (i.e. $B_{\mathrm{L}} = 0$) in a ΛCDM model with no tensors. In Fig. 1 the contribution of each of the integrals appearing in Eq. (4.26) is illustrated. The analytical form of these integrals has been derived in Eqs. (4.27), (4.28), (4.29) and (4.30). In Fig. 1 (plot at the left) the separate con-

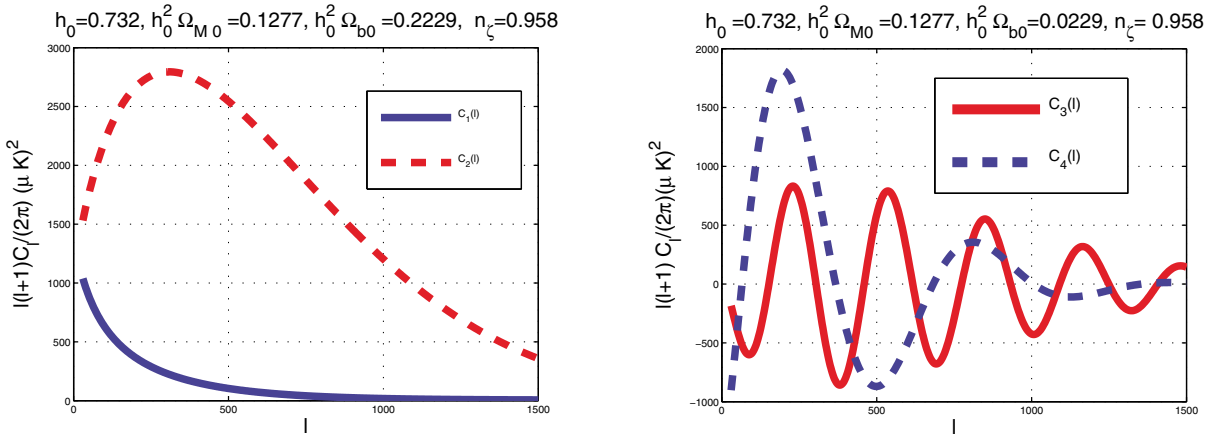

Figure 1
The contribution of each of the integrals giving the temperature autocorrelations is reported (see Eq. (4.26)). The parameters are chosen in such a way to match the best fit to the experimental points when only the WMAP data are included and the contribution of the tensor modes is assumed to be vanishing.

tributions of $\ell(\ell + 1)\, C_1(\ell)/(2\pi)$ and of $\ell(\ell + 1)C_2(\ell)/(2\pi)$ have been reported for a fiducial set of parameters (i.e. $n_\zeta = 0.958$, $h_0^2\Omega_{M0} = 0.1277$ and $h_0^2\Omega_{b0} = 0.0229$). This fiducial set of parameters corresponds to the best fit of the WMAP 3-year data alone [1]. As mentioned in Eq. (3.49) the pivot wave-number is $k_p = 0.002$ Mpc^{-1}. This is also the choice made by WMAP team. In the plot at the right (always in Fig. 1) the separate contributions of $\ell(\ell + 1)C_3(\ell)/(2\pi)$ and of $\ell(\ell + 1)C_4(\ell)/(2\pi)$ is illustrated for the same fiducial set of parameters (which is also described at the top of the plot). The various contributions are expressed in units of $(\mu\mathrm{K})^2$ (i.e. $1\mu\mathrm{K} = 10^{-6}\mathrm{K}$) which are the appropriate ones for the comparison with the data. The normalization of the calculation is set by evaluating (analytically) the large-scale contribution for $\ell < 30$ (see Eq. (3.45)) and by comparing it, in this region, with the WMAP 3-year data release.

By summing up the four separate contributions illustrated in Fig. 1, Eq. (4.26) allows to determine, for a given choice of cosmological parameters, the full temperature autocorrelations. The results, always in the absence of magnetized contribution, are reported in Fig. 2. In the plot at the left of Fig. 2 the critical fractions of matter and baryons, as well as h_0, are all fixed. The only quantity allowed to vary from one curve to the other is the scalar spectral index of curvature perturbations, i.e. n. The full line denotes the pivot case $n_\zeta = 0.958$ (corresponding to the central value for the spectral index as determined according to the WMAP data alone). The dashed and dot-dashed lines correspond, respectively, to $n_\zeta = 0.974$ and $n_\zeta = 0.942$ (which define the allowed range of n since $n_\zeta = 0.958 \pm 0.016$ [1]).

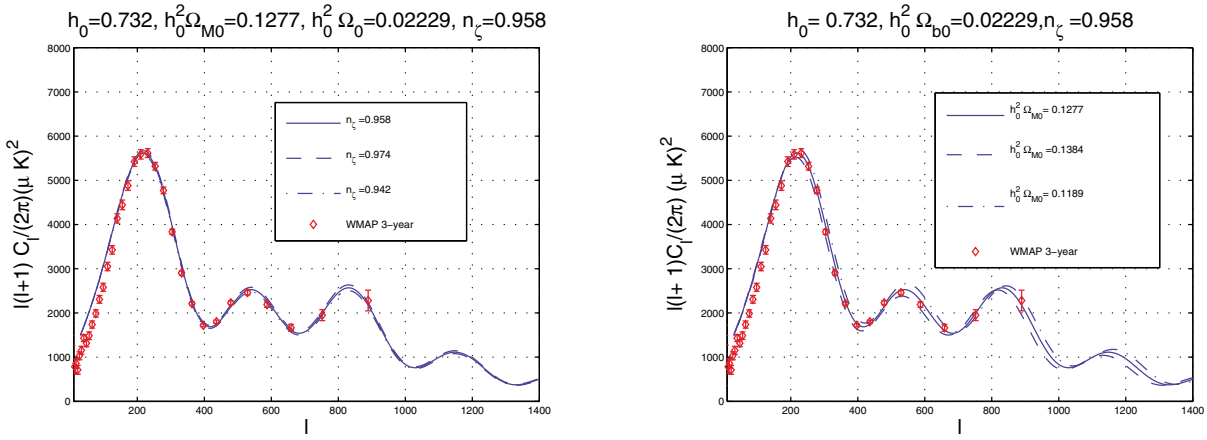

Figure 2
The temperature autocorrelations for a fiducial set of cosmological parameters chosen within a concordance model and in the case $B_L = 0$.

As already stressed, the regime $\ell < 100$ is only reasonably reproduced while the most interesting region, for the present purposes, is rather accurate (as the comparison with the WMAP data shows). The region of very large ℓ (i.e. $\ell > 1200$) is also beyond the treatment of diffusive effects adopted in the present paper. In Figure 2 (plot at the right) the adiabatic spectral index is fixed (i.e. $n_\zeta = 0.958$) while the total (present) fraction of non-relativistic matter is allowed to vary (h_0 and $h_0^2\Omega_{b0}$ are, again, kept fixed). It can be observed that, according to Fig. 2, the amplitude of the first peak increases as the total (dusty) matter fraction decreases.

The contribution of the magnetic fields will now be included both in the Sachs-Wolfe region (as discussed in section 3) and in the Doppler region (as discussed in section 4). In Fig. 3 the temperature autocorrelations are computed in the presence of a magnetized background. The values of the relevant magnetic parameters (i.e. the smoothed amplitude of the field B_L and the spectral slope ε) are reported at the top of each plot and in the legends. In the plot at the left of Fig. 3 the spectral slope is fixed as $\varepsilon = 0.01$ while B_L is allowed to vary. The other cosmological parameters are fixed to their concordance values stemming from the analysis of the WMAP 3-year data and are essentially the ones already reported at the top of Fig. 2. The diamonds are the WMAP 3-year data points. In the plot at the right of Fig. 3 the spectral slope is still reasonably flat but, this time, $\varepsilon = 0.1$. For a spectral slope $\varepsilon = 0.01$ the case $B_L = 1$nG is barely distinguishable (but not indistinguishable, as we shall see below) from the case $B_L = 0$. As soon as B_L increases from 1 to 5 nG three different phenomena take place:

• the first Doppler peak increases dramatically and it reaches a value of the order of 1.2×10^4 $(\mu K)^2$ when $B_L = 2$ nG;

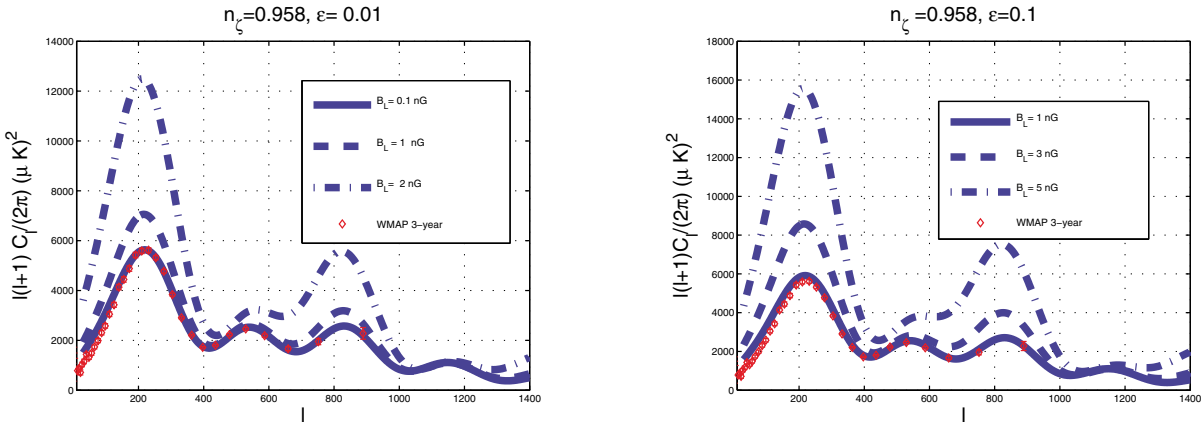

Figure 3
The inclusion of the effects of large-scale magnetic fields in the case of nearly scale-invariant magnetic energy spectrum (i.e. $0 < \varepsilon < 1$). The conventional adiabatic spectral index is fixed to the same value assumed in the right plot of Fig. 2.

• already for 0.1 nG $< B_{\rm L} <$ 2 nG the third peak increases while the second peak becomes less pronounced;

• as soon as $B_{\rm L} \geq 2$ nG the second peak practically disappears and it is replaced by a sort of hump.

If the spectral slope increases a similar trend takes place as $B_{\rm L}$ increases. However, the formation of the hump takes place for values of $B_{\rm L}$ which are comparatively larger than in the case of nearly scale-invariant magnetic energy spectrum. In Fig. 3 (plot at the right) the magnetic spectral slope is $\varepsilon = 0.1$ (while the adiabatic spectral slope is fixed to the concordance value, i.e. $n_\zeta = 0.984$). To observe the formation of the hump (which is of course excluded by experimental data) the values of $B_{\rm L}$ must be larger and in the range of 15 to 20 nG. As soon as ε increases towards 1 the minimal allowed $B_{\rm L}$ also increases. This is particularly evident from the two plots reported in Fig. 4 where the values of ε have been chosen to be 0.5 (plot at the left) and 0.9 (plot at the right).

In Fig. 4 the dashed curve in the plot at the right corresponds to $B_{\rm L} = 6$ nG. For this value of $B_{\rm L}$ the hump is not yet present, while for $\varepsilon = 0.01$ already for $B_{\rm L} = 2$nG the second peak is completely destroyed. These differences are related to the fact that an increase in ε implies, indirectly, that the amplitude of the power spectrum of the magnetized background decreases at large length-scales, i.e. for small wave-numbers. From Fig. 3 it can be argued, for instance, that when the magnetic slope is nearly flat (i.e. $\varepsilon \simeq 0.01$), the allowed value of the smoothed field becomes $B_{\rm L} < 0.1$ nG. It should be remarked, to avoid confusion, that the scale invariant limit for the curvature perturbations, according to the conventions of the present paper is $n_\zeta \to 1$ while the scale invariant

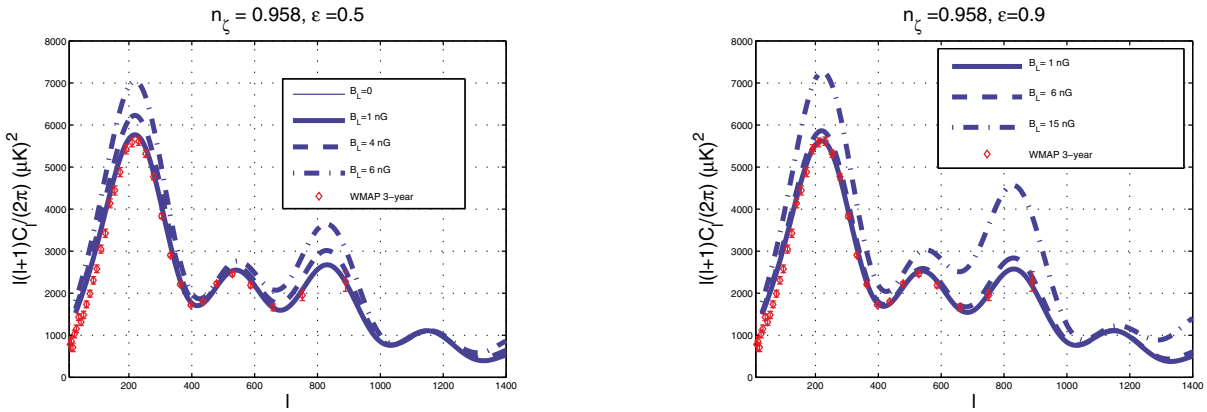

Figure 4
The inclusion of the effects related to laarge-scale magnetization in the case of a blue magnetic spectral index.

limit for the magnetic energy density fluctuations is $\varepsilon << 1$. Finally in Fig. 5 the effect of the variation of the magnetic pivot scale is illustrated. If k_L diminishes by one order of magnitude the temperature autocorrelations increase in a different way depending upon the value of ε. By diminishing k_L the magnetic field is smoothed over a larger length-scale. The net effect of this choice will be to increase the temperature autocorrelations for the same values of B_L and ε.

For $\ell = 210$ the experimental value of the temperature autocorrelations is [1-3] 5586 ± 106.25 $(\mu K)^2$, while for $\ell = 231$ the experimental value is 5616.35 ± 99.94 $(\mu K)^2$. The next value, i.e. $\ell = 253$ implies 5318.06 ± 86.19 $(\mu K)^2$. By requiring that the addition of the magnetic field does not shift appreciably the height of the first Doppler peak it is possible to find, for each value of the spectral slope ε a maximal magnetic field which approximately coincides, in the cases of Fig. 3 with the lowest curve of each plot. This argument is sharpened in Fig. 6 where the starred points represent the computed values of the temperature autocorrelations for two different values of B_L

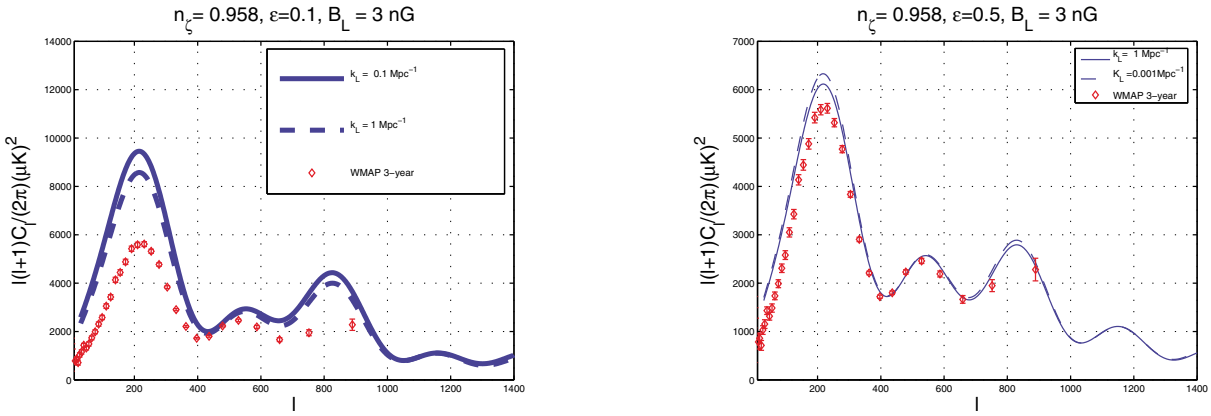

Figure 5
The variation of the magnetic pivot scale is illustrated for two different spectral slopes.

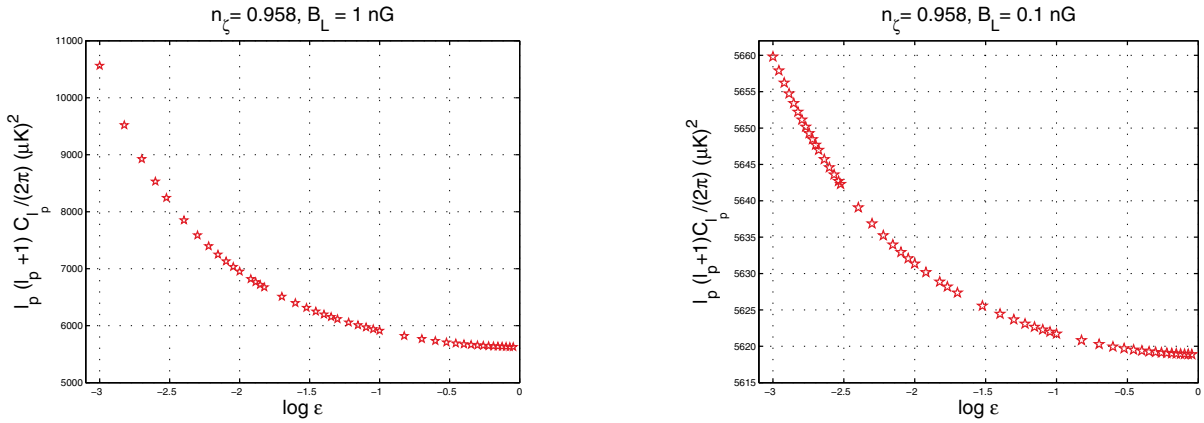

Figure 6
The stars represents the points obtained by numerical integration. On the vertical axis, in both plots, the (computed) value of the temperature autocorrelations at the first Doppler peak (i.e. $\ell = \ell_p$) is reported as a function of the magnetic spectral slope for two values of the smoothed magnetic field intensity.

and for the interesting range of ε. The value of ℓ_p, i.e. the multipole corresponding to the first Doppler peak, has been taken, according to [1-3] to be 220. If, according to experimental data, the following condition

$$\left[\frac{\ell_p(\ell_p+1)C_{\ell_p}}{2\pi}\right]_{\text{computed}} \leq 5260(\mu K)^2 \tag{5.1}$$

is enforced, then, the smoothed field intensity and the spectral slope will be bounded in terms of the position and height of the Doppler peak. This condition is indeed sufficient since, according to the numerical results reported in the previous figures, the distortion of the second and third peaks are always correlated with the increase of the first peak. Already at a superficial level, it is clear that if $B_L \leq 1$nG the only spectral slopes compatible with the requirement of Eq. (5.1) are rather blue and, typically $\varepsilon > 0.5$. The numerical values obtained with the method described in Fig. 6 are well represented by the following interpolating formula

$$\left[\frac{\ell_p(\ell_p+1)C_{\ell_p}}{2\pi}\right]_{\text{computed}} = \left[\left(\frac{B_L}{\text{nG}}\right)^2 \frac{c_1}{\log \varepsilon^{c_2}+1} + 5617\right](\mu\text{K})^2, \quad c_1 = 46.71, \quad c_2 = 0.55, \tag{5.2}$$

which holds for $B_L \leq$ nG a bit less accurate in the region $B_L >$ nG which is already excluded by inspection of the shape of the temperature autocorrelations. By then comparing the value of the

temperature autocorrelations in the location of the first Doppler peak the amplitude of the magnetic field can therefore be bounded. In particular it is easy to show that

$$\left(\frac{B_{\rm L}}{\rm nG}\right)^2 \leq \frac{1}{c_1}\left(\frac{\sqrt{\Delta_{\rm p}}}{\mu{\rm K}}\right)^2 \log[\varepsilon^{c}2+1], \tag{5.3}$$

where

$$\Delta_{\rm p}=\left[\frac{\ell_{\rm p}(\ell_{\rm p}+1)C_{\ell_{\rm p}}}{2\pi}\right]_{\rm measured} -5617(\mu{\rm K})^2. \tag{5.4}$$

The quantity $\Delta_{\rm p}$ is known once the experimental determination of the height of the peak is available. Consequently, by determining experimentally the value of the temperature autocorrelations at the first Doppler peak located for a multipole $\ell_{\rm p}$ the magnetic field intensity and the spectral slope will be bounded according to Eq. (5.4). If, as WMAP data suggest, we take $\Delta_{\rm p} = 3(\mu{\rm K})^2$, the bounds on $B_{\rm L}$ and ε are illustrated in Fig. 7.

Thus, according to the results described so far it is possible to say that to avoid gross distortion of the temperature autocorrelations attributed to large-scale magnetic fields we have to demand that the stochastic field satisfies

$$B_{\rm L} \leq 0.08{\rm nG}, \quad 0.001 \leq \varepsilon < 1 \tag{5.5}$$

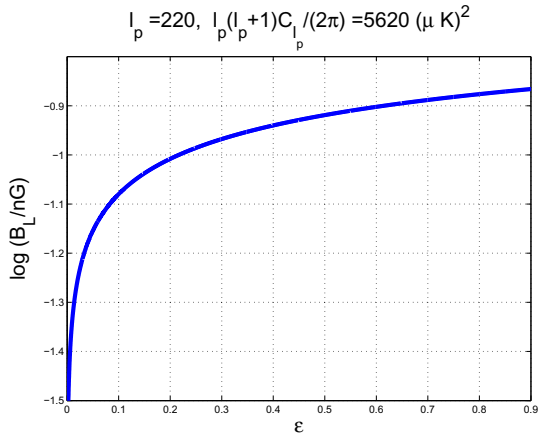

Figure 7
Allowed region (below the thick curve) in the plane ($B_{\rm L}$, ε) for $\ell_{\rm p}$ = 220 and for $\Delta_{\rm p} = 3(\mu{\rm K})^2$.

If a magnetic field with smoothed amplitude $B_{\rm L} \leq 0.1$ nG is present before recombination the implication for the formation of magnetized structures are manifold. We recall that the value $B_{\rm L}$ is the smoothed magnetic field redshifted at the epoch of the gravitational collapse of the proto-galaxy. We know that, during collapse, the freezing of magnetic flux justifies the compressional amplification of the pre-existing field that will be boosted by roughly four orders of magnitude during the collapse [15]. This will bring the amplitude of the field to the μG level. It is however premature to speculate on these issues. There are, at the moment, two important steps to be undertaken:

• the forthcoming PLANCK explorer data will allow to strengthen the constraints derived in the present paper and, in particular, the formulae derived in the present section will allow to constraint directly the possible magnetized distortions stemming from the possible presence of large-scale magnetic fields;

• another precious set of informations may come from the analysis of the magnetic fields in clusters and superclusters; it would be interesting to know, for instance, which is the spectral slope of the magnetic fields in galaxies, clusters and superclusters.

The other interesting suggestion of the present analysis is that the inclusion of a large-scale magnetic field as a fit parameter in an extended ΛCDM model is definitely plausible. The ΛCDM model has been extended to include, after all, different possibilities like the ones arising in the dark-energy sector. Here we have the possibility of adding the parameters of a magnetized background which are rather well justified on the physical ground. Notice, in particular, that interesting degeneracies can be foreseen. For instance, the increase of the first peak caused by a decrease in the dark-matter fraction can be combined with the presence of a magnetic field whose effect, as we demonstrated, is to shift the first Doppler peak upwards. These issues are beyond the scopes of the present paper.

6 Concluding remarks

There are no compelling reasons why large-scale magnetic fields should not be present prior to recombination. In this paper, via a semi-analytical approach, the temperature autocorrelations induced by large-scale magnetic fields have been computed and confronted with the available experimental data. Of course the data analysis can be enriched by combining the WMAP data also with other data sets and by checking the corresponding effects of large-scale magnetic fields. The main spirit of this investigation was, however, not to discuss the analysis of data but to show that the effects of large-scale magnetic fields on the temperature autocorrelations can be brought at the same theoretical standard of the calculations that are usually performed in the absence of magnetic fields.

According to this perspective it is interesting to notice that, at the level of the pre-equality initial conditions, the presence of magnetic field induces a quasi-adiabatic mode. Depending on the features of the magnetic spectrum (i.e. its smoothed amplitude $B_{\rm L}$ and its spectral slope ε), possible distortions of the first and second peaks can jeopardize the shape of the observed temperature autocorrelations. In particular, for sufficiently strong magnetic backgrounds (i.e. $B_{\rm L} > 10$ nG and $\varepsilon \leq 0.3$), the second peak turns into a hump. From the analysis of these distortions it was possible to derive a bound that depends solely upon measurable quantities such as the location of the first peak and its height. The derived formulae will allow a swifter comparison of the possible effects of large-scale magnetic fields with the forthcoming experimental data such as the ones of PLANCK explorer. The available WMAP data suggest that $B_{\rm L} \leq 0.08$ nG for $0.001 \leq \varepsilon < 1$. This range of parameters does not exclude that magnetic fields present prior to recombination could be the seeds of magnetized structures in the sky such as galaxies, clusters and superclusters. It is also interesting to remark that the allowed range of parameters does not exclude the possibility that the magnetic field of galaxies is produced from the pre-recombination field even without a strong dynamo action whose possible drawbacks and virtues are, at present, a subject of very interesting debates.

In recent years CMB data have been confronted with a variety of cosmological scenarios that take as a pivotal model the ΛCDM paradigm. Some of the parameters usually added encode informations stemming from effects that, even if extremely interesting, arise at very high energy and curvature scales. While it is certainly important to test any predictive cosmological scenario, we would like to stress that the purpose of the present work is, in some sense, more modest. We hope to learn from CMB not only what was the initial state of the Universe when the Hubble rate was only one millionth times smaller than the Planck (or string) mass scale; if possible we would like to learn from CMB how and why the largest magnetized structures arose in the sky. Since we do see magnetic fields today it is definitely a well posed scientific question to know what were their effects prior to recombination. It would be desirable, for instance, to find clear evidence of the absence of pre-recombination magnetic fields. It would be equally exciting to determine the possible presence of this natural component. It is therefore opinion of the author that the inclusion of a magnetized component in future experimental studies of CMB observables represents a physically motivated option which we do hope will be seriously considered by the various collaborations which are today active in experimental cosmology.

A Magnetized gravitational perturbations

In this Appendix the evolution equations of the magnetized curvature perturbations will be presented in the conformally Newtonian gauge where the only two non vanishing components of the perturbed metric are

$$\delta_{\rm s} g_{00}(\tau,\vec{x}) = 2a^2(\tau)\phi(\tau,\vec{x}), \quad \delta_{\rm s} g_{ij}(\tau,\vec{x}) = 2a^2(\tau)\psi(\tau,\vec{x})\delta_{ij}, \tag{A.1}$$

where δ_s signifies the scalar nature of the fluctuation. While these equations are available in the literature [34,35], it seems appropriate to give here an explicit and reasonably self-contained treatment of some technical tools that constitute the basis of the results reported in the bulk of the paper.

The magnetic fields are here treated in the magnetohydrodynamical (MHD) approximation where the displacement current is neglected and where the three dynamical fields of the problem (i.e., respectively, the magnetic field, the Ohmic electric field and the total Ohmic current) are all solenoidal. The bulk velocity field, in this approach, is given by the centre of mass velocity of the electron-proton system. This is physically justified since electrons and protons are strongly coupled by Coulomb scattering. Photons and baryon are also strongly coupled by Thompson scattering, at least up to recombination which is the relevant time-scale for the effects of magnetic fields on temperature autocorrelations. The bulk velocity of the plasma can be separated into an irrotational part and into a rotational part which contributes to the evolution of the vector modes of the geometry [27]. In the present investigation only the scalar modes are treated and, therefore, only the irrotational part of the velocity field will be relevant. In the MHD approach the magnetic fields enter, both, the perturbed Einstein equations and the Boltzmann hierarchy.

A.1 Perturbed Einstein equations

The perturbed Einstein equations are affected by the various components of the (perturbed) energy-momentum. The contribution of the magnetic fields to the scalar fluctuations of the energy-momentum tensor are:

$$\delta_{\rm s}\mathcal{T}^0_0=\delta\rho_{\rm B}=\frac{B^2(\tau,\vec{x})}{8\pi a^4(\tau)},\quad \delta_{\rm s}\mathcal{T}^j_i=-\delta p_{\rm B}\delta^j_i+\tilde{\Pi}^j_i,\quad \delta p_{\rm B}=\frac{\delta\rho_{\rm B}}{3}, \tag{A.2}$$

where

$$\tilde{\Pi}^j_i=\frac{1}{4\pi a^4}\left[B_iB^j-\frac{1}{3}B^2\delta^j_i\right], \tag{A.3}$$

is the magnetic anisotropic stress. Using the practical notation[15] is $\partial_i\partial^j\tilde{\Pi}^i_j=(p_\gamma+\rho_\gamma)\nabla^2\sigma_{\rm B}$ the spatial (and traceless) components of the perturbed Einstein equations imply

$$\nabla^4(\phi - \psi) = 12\pi G a^2[p_\nu+\rho_\nu)\nabla^2\sigma_\nu+(p_\gamma+\rho_\gamma)\nabla^2\sigma_{\rm B}], \tag{A.4}$$

where σ_ν is the neutrino anisotropic stress. The Hamiltonian and momentum constraints can then be written as

$$\nabla^2\psi - 3\mathcal{H}(\mathcal{H}\phi + \psi') = 4\pi G a^2(\delta\rho_{\rm t} + \delta\rho_{\rm B}), \tag{A.5}$$

$$\nabla^2(\mathcal{H}\phi + \psi') = -4\pi G a^2(p_{\rm t} + \rho_{\rm t})\theta_{\rm t}, \tag{A.6}$$

where $\delta_{\rho{\rm t}} = \sum_a \delta_{\rho a}$ is the total density fluctuation (with the sum running over the four species of the plasma, i.e. photons, baryons, neutrinos and CDM particles). Equations (A.5) and (A.6) are simply derived from the perturbed components of the (00) and (0*i*) Einstein equations [34,35] (see also [13] for a comparison with the conventional situation where magnetic fields are absent). Notice that the MHD Pointying vector has not been included in the momentum constraint. The rationale for this approximation stems from the fact that this contribution is proportional to $\vec{\nabla}\cdot(\vec{E}\times\vec{B})$ and it contains one electric field which is suppressed, in MHD, by one power of $\sigma_{\rm c}$, i.e. the Ohmic conductivity.

In Eq. (A.6) $\theta_{\rm t}$ is the three-divergence of the total peculiar velocity, i.e.

$$(p_{\rm t} + \rho_{\rm t})\theta_{\rm t} = \frac{4}{3}\rho_\nu\theta_\nu + \rho_{\rm c}\theta_{\rm c} + \frac{4}{3}\rho_\gamma(1 + R_{\rm b})\theta_{\gamma{\rm b}}, \tag{A.7}$$

where $\theta_{\gamma{\rm b}}$ is the baryon-photon velocity and $R_{\rm b}$ is baryon-photon ratio defined in Eq. (2.10). In particular, at recombination,

$$R_{\rm b}(z_{\rm rec}) = 0.664\left(\frac{h_0^2\Omega_{\rm b0}}{0.023}\right)\left(\frac{1051}{z_{\rm rec}+1}\right). \tag{A.8}$$

Finally from the spatial components of the perturbed Einstein equations we get

$$\psi'' + \mathcal{H}(\phi' + 2\psi') + (2\mathcal{H}' + \mathcal{H}^2)\phi + \frac{1}{3}\nabla^2(\phi - \psi) = 4\pi G a^2(\delta p_{\rm t} + \delta p_{\rm B}). \tag{A.9}$$

The evolution equations of the metric fluctuations can be also usefully supplemented by the covariant conservation of the total density fluctuation of the fluid which can be written as

$$\delta\rho_{\rm t}' + 3\mathcal{H}(\delta\rho_{\rm t} + \delta p_{\rm t}) + (p_{\rm t} + \rho_{\rm t})\psi' + (p_{\rm t} + \rho_{\rm t})\theta_{\rm t} = 0. \tag{A.10}$$

This form of the total conservation equation allows to find rather swiftly the evolution equations of the gauge-invariant density contrast ζ. The evolution equation of the total velocity field of the mixture can also be obtained from the covariant conservation of the total energy-meomentum tensor

$$(p_{\rm t}+\rho_{\rm t})\theta_{\rm t}+[(p_{\rm t}'+\rho_{\rm t}')+4\mathcal{H}(p_{\rm t}+\rho_{\rm t})]+\nabla^2\delta p_{\rm t}+(p_{\rm t}+\rho_{\rm t})\nabla^2\phi+\frac{4}{3}\eta\nabla^2\theta_{\rm t}=0, \tag{A.11}$$

where η denotes the shear viscosity coefficient which is particularly relevant for the baryon-photon system and which is related to the photon mean free path (see below in this Appendix).

A.2 Different fluids of the mixture

The relevant equations will now be written directly in Fourier space omitting the explicit reference to the wave-number since the subscript may be confused with the other subscripts labeling each species of the fluid. The evolution of CDM particles is rather simple since it is only sensitive to the fluctuation of the metric:

$$\delta_{\rm c}'=3\psi'-\theta_{\rm c}, \tag{A.12}$$

$$\theta_{\rm c}'+\mathcal{H}\theta_{\rm c}=k^2\phi. \tag{A.13}$$

Defining the gauge-invariant density contrast of CDM, i.e. $\zeta_c = -\psi + \delta_c/3$, it is immediate to combine Eqs. (A.12) and (A.13) and obtain:

$$\zeta_{\rm c}''+\mathcal{H}\zeta_{\rm c}=-\frac{k^2}{3}\phi, \tag{A.14}$$

whose solution is

$$\zeta_{\rm c}(\tau,k)=\zeta(\tau_{\rm i},k)-\frac{k^2}{3}\int_{\tau_{\rm i}}^{\tau}\frac{d\tau''}{a(\tau'')}\int_{\tau_{\rm i}}^{\tau''}\phi(k,\tau')a(\tau')d\tau', \tag{A.15}$$

where $\tau_{\rm i}$ is the initial integration time. In terms of the CDM density contrast and in the limit of vanishing anisotropic stress

$$\delta_{\rm c}(\tau,k)=\delta_{\rm c}(\tau_{\rm i},k)+3(\phi(\tau,k)-\phi(\tau_{\rm i},k))-k^2\int_{\tau_{\rm i}}^{\tau}\frac{d\tau''}{a(\tau'')}\int_{\tau_{\rm i}}^{\tau''}\phi(k,\tau')a(\tau')d\tau' \tag{A.16}$$

The lowest multipoles of the neutrino hierarchy lead to the following set of equations where the contribution of the quadrupole (i.e. $2\sigma_\nu$) and octupole (i.e. $\mathcal{F}_{\nu 3}$) have been explicitly included:

$$\delta'_\nu = 4\psi' - \frac{4}{3}\theta_\nu, \tag{A.17}$$

$$\theta'_\nu = \frac{k^2}{4}\delta_\nu - k^2\sigma_\nu + k^2\phi, \tag{A.18}$$

$$\sigma'_\nu = \frac{4}{15}\theta_\nu - \frac{3}{10}\mathcal{F}_{\nu 3}. \tag{A.19}$$

Unlike neutrinos and CDM particles that feel the effect of the magnetic fields through the anisotropic stress and through the metric fluctuations, the photons, being tightly coupled with the baryons by Thompson scattering, are directly affected by the presence of large-scale magnetic fields. Let us clarify this point by writing, separately, the relevant evolution equations for the photons and their counterpart for the baryons. In real space the evolution equations of the photons can be written as:

$$\delta'_\gamma = 4\psi' - \frac{4}{3}\theta_\gamma, \tag{A.20}$$

$$\theta'_\gamma = -\frac{1}{4}\nabla^2\delta_\gamma - \nabla^2\phi + \varepsilon'(\theta_{\rm b} - \theta_\gamma), \tag{A.21}$$

where ε' is the inverse of the photon mean free path. The baryon evolution equations are:

$$\delta'_{\rm b} = 3\psi' - \theta_{\rm b}, \tag{A.22}$$

$$\theta'_{\rm b} + \mathcal{H}\theta_{\rm b} = -\nabla^2\phi + \frac{4}{3}\frac{\rho_\gamma}{\rho_{\rm b}}\varepsilon'(\theta_\gamma - \theta_{\rm b}) + \frac{\vec{\nabla}\cdot[\vec{J}\times\vec{B}]}{a^4\rho_{\rm b}}, \tag{A.23}$$

where $\vec{J}\times\vec{B}$ is the MHD Lorentz force. Equations (A.21) and (A.23) can now be summed and subtracted after having multiplied Eq. (A.23) by $R_{\rm b}$. By subtracting the two aforementioned equations, we will obtain an equation for (θ_γ- $\theta_{\rm b}$) whose solution will imply a strong damping leading, in spite of the initial conditions, to $\theta_\gamma \simeq \theta_{\rm b} = \theta_{\gamma{\rm b}}$. From the sum of Eqs. (A.21) and (A.23) the evolution equation of $\theta_{\gamma{\rm b}}$will then be directly obtained. In the tight coupling limit the evolution equations of the magnetized baryon-photon system is, therefore [34]:

$$\delta'_\gamma = 4\psi' - \frac{4}{3}\theta_{\gamma{\rm b}}, \tag{A.24}$$

$$\theta'_{\gamma \mathrm{b}} + \frac{\mathcal{H} R_{\mathrm{b}}}{1+R_{\mathrm{b}}}\theta_{\gamma \mathrm{b}} + \frac{\eta}{\rho_{\gamma}(R_{\mathrm{b}}+1)}k^2\theta_{\gamma \mathrm{b}} = \frac{k^2}{4(1+R_{\mathrm{b}})}\delta_{\gamma} + k^2\phi + \frac{k^2(\Omega_{\mathrm{B}}-4\sigma_{\mathrm{B}})}{4(1+R_{\mathrm{b}})}, \quad (A.25)$$

$$\delta'_{\mathrm{b}} = 3\psi' - \theta_{\gamma \mathrm{b}}, \quad (A.26)$$

where

$$\eta = \frac{4}{15}\rho_{\gamma}\lambda_{\mathrm{T}}, \quad (A.27)$$

is the shear viscosity coefficient that leads to the Silk damping of the high harmonics in the CMB temperature autocorrelations. The important identity (heavily used in this algebra) is

$$\frac{3}{4a^4\rho_{\gamma}}\vec{\nabla}\cdot[\vec{J}\times\vec{B}] = \nabla^2\sigma_{\mathrm{B}} - \frac{1}{4}\nabla^2\Omega_{\mathrm{B}}. \quad (A.28)$$

This identity can be swiftly derived by recalling Eq. (A.4) and by using two further vector identities:

$$\vec{\nabla}\cdot[\vec{J}\times\vec{B}] = \frac{1}{4\pi}\vec{\nabla}\cdot[(\vec{\nabla}\times\vec{B})\times\vec{B}], \quad \partial_i B_j \partial^j B^i = \vec{\nabla}\cdot[(\vec{\nabla}\times\vec{B})\times\vec{B}] + \frac{1}{2}\nabla^2 B^2. \quad (A.29)$$

The relation between the magnetic anisotropic stress and σ_{B} has been introduced before (i.e. after Eq. (A.4)) and it is simply $\partial_j\partial^i\tilde{\Pi}^j_i = \nabla^2\sigma_{\mathrm{B}}$. Defining the gauge-invariant density contrast for the photons, i.e. $\zeta_{\gamma} = -\psi + \delta_{\gamma}/4$ and combining Eqs. (A.24), (A.25) and (A.26) the following simple equation can be readily obtained:

$$\zeta''_{\gamma} + \frac{\mathcal{H} R_{\mathrm{b}}}{R_{\mathrm{b}}+1}\zeta'_{\gamma} + \frac{4}{15}k^2\frac{\lambda_{\mathrm{T}}}{R_{\mathrm{b}}+1}\zeta'_{\gamma} + \frac{k^2}{3(R_{\mathrm{b}}+1)}\zeta_{\gamma} = -\frac{k^2}{3}\left[\phi + \frac{\psi}{R_{\mathrm{b}}+1}\right] + \frac{k^2}{12(R_{\mathrm{b}}+1)}(4\sigma_{\mathrm{B}} - \Omega_{\mathrm{B}}). \quad (A.30)$$

By now defining the photon-baryon sound speed c_{sb} we have

$$c_{\mathrm{sb}} = \frac{1}{\sqrt{3(R_{\mathrm{b}}+1)}}, \quad \frac{(c^2_{\mathrm{sb}})'}{c^2_{\mathrm{sb}}} = -\frac{\mathcal{H} R_{\mathrm{b}}}{R_{\mathrm{b}}+1}, \quad (A.31)$$

which also implies, when inserted into Eq. (A.30), that

$$\zeta_{\gamma}'' - \frac{(c_{\rm sb}^2)'}{c_{\rm sb}^2}\zeta_{\gamma}' + \frac{4}{5}k^2 c_{\rm sb}^2 \lambda_{\rm T}\zeta_{\gamma}' + k^2 c_{\rm sb}^2 = -\frac{k^2}{3}(\phi + 3c_{\rm sb}^2\psi) + \frac{k^2}{4}c_{\rm sb}^2(4\sigma_{\rm B} - \Omega_{\rm B}). \tag{A.32}$$

By now changing variable from the conformal time coordinate τ to $dq = c_{\rm sb}^2 d\tau$, Eq. (A.32) becomes:

$$\frac{d^2\zeta_{\gamma}}{dq^2} + \frac{4}{5}k^2\lambda_{\rm T}\frac{d\zeta_{\gamma}}{dq} + \frac{k^2}{c_{\rm sb}^2}\zeta_{\gamma} = -\frac{k^2}{3c_{\rm sb}^4}(\phi + 3c_{\rm sb}^2\psi) + \frac{k^2}{4c_{\rm sb}^2}(4\sigma_{\rm B} - \Omega_{\rm B}). \tag{A.33}$$

The solution of the homogeneous equation can be simply obtained in the WKB approximation [39,42,43,45] and it is

$$\zeta_{\gamma}(\tau, k) = \frac{1}{\sqrt{3(R_{\rm sb}+1)}}\{C_1\cos[\alpha(\tau,k)] + C_2\sin[\alpha(\tau,k)]\}e^{-\frac{k^2}{k_{\rm D}^2}}, \tag{A.34}$$

where the quantities appearing in Eq. (A.34) are:

$$\frac{1}{k_{\rm D}^2(\tau)} = \frac{2}{5}\int_0^{\tau} c_{\rm sb}(\tau')\frac{a_0 d\tau'}{a(\tau')x_{\rm e}n_{\rm e}\sigma_{\rm T}}, \tag{A.35}$$

$$\alpha(\tau, k) = k\int^{\tau} c_{\rm sb}(\tau')d\tau'. \tag{A.36}$$

Since $\delta_{\gamma} = 4(\zeta_{\gamma} + \psi)$, Eqs. (A.33), (A.34) can also be used to determine the photon density contrast which is a key ingredient for the estimate of the temperature autocorrelations both at large and small angular scales.

A.3 Evolution of the brightness perturbations

The evolution equations of the brightness perturbations can be easily derived within the set of conventions employed in the present paper. Recalling that $\theta_{\rm b}$ is the divergence of the peculiar velocity field of the baryons, it is convenient to define, for notational convenience, $v_{\rm b}$ i.e.

$$v_{\rm b} = \frac{\theta_{\rm b}}{ik} \simeq \frac{\theta_{\gamma {\rm b}}}{ik}, \tag{A.37}$$

where the second equality holds in the tight coupling approximation. From Eq. (A.23) it then follows that the evolution of $v_{\rm b}$ is simply given by

$$v'_{\rm b} + \mathcal{H} v_{\rm b} + ik\phi + \frac{\varepsilon'}{R_{\rm b}}\left(3i\Delta_{\rm I1} + v_{\rm b}\right) = \frac{ik}{4R_{\rm b}}(\Omega_{\rm B} - 4\sigma_{\rm B}), \tag{A.38}$$

having used that $\theta_\gamma = 3k\Delta_{\rm I1}$ which simply reflects the occurrence that the dipole of the intensity of the perturbed radiation field is related to the peculiar velocity of the photons once the fluctuation of the intensity is expanded in multipoles as

$$\Delta_{\rm I}(\vec{k}, n, \tau) = \sum_{\ell} (-i)^{\ell} (2\ell + 1) \Delta_{{\rm I}\ell}(k, \tau) P_{\ell}(\mu), \tag{A.39}$$

where $\hat{n}$ is the direction of the momentum of the photon, $\mu = \hat{n} \cdot \hat{k}$ and $P\ell(\mu)$ are the Legendre polynomials of index ℓ and argument μ. Analog expansion hold for the brightness perturbations related with the other two Stokes parameters, i.e. Q and U. It should be remarked, incidentally, that the ℓ-dependent factors appearing in Eq. (A.39) are conventional. If different conventions in the expansion are adopted, the various expressions of the multipoles will change accordingly. With these necessary specifications we have that

$$\Delta'_{\rm I} + (ik\mu + \varepsilon')\Delta_{\rm I} = \psi' - ik\mu\phi + \varepsilon'\left[\Delta_{\rm I0} + \mu v_b - \frac{1}{2} P_2(\mu) S_{\rm Q}\right], \tag{A.40}$$

$$\Delta'_{\rm Q} + (ik\mu + \varepsilon')\Delta_{\rm Q} = \frac{\varepsilon'}{2}[1 - P_2(\mu)] S_{\rm Q}\Big\}, \tag{A.41}$$

$$\Delta'_{\rm U} + (ik\mu + \varepsilon')\Delta_{\rm U} = 0, \tag{A.42}$$

where we defined, for notational convenience

$$S_{\rm Q} = \Delta_{\rm I2} + \Delta_{\rm Q0} + \Delta_{\rm Q2}. \tag{A.43}$$

In Eqs. (A.41)–(A.42), $P_2(\mu) = (3\mu^2 - 1)/2$ is the Legendre polynomial of second order, which appears in the collision operator of the Boltzmann equation for the photons due to the directional nature of Thompson scattering. Since we shall be chiefly concerned with the temperature autocorrelations, let us remind that, using the technique of integration along the line of sight, Eq. (A.40) can be solved, after integration by parts, as

$$\Delta_{\rm I}(\vec{k}, \tau_0) = \int_0^{\tau_0} e^{-\varepsilon(\tau, \tau_0)}(\psi' + \phi') + \int_0^{\tau_0} \mathcal{K}(\tau)\left[\Delta_{\rm I0} + \phi + \mu v_{\rm b} - \frac{1}{2} P_2(\mu) S_{\rm Q}\right] e^{-i\mu k(\tau_0 - \tau)}, \tag{A.44}$$

where $\mathcal{K} = \varepsilon' e^{-\varepsilon}$ is the visibility function. In the sudden recombination approximation, relevant for wavelengths larger that the Hubble radius we will have that, according to Eq. (A.44) the Sachs-Wolfe contribution and the integrated Sachs-Wolfe contribution are simply given by

$$\Delta_{\mathrm{I}}^{(\mathrm{SW})}(\vec{k},\tau_0)=\Delta_{\mathrm{I}0}(\vec{k},\tau_{\mathrm{rec}})+\phi(\vec{k},\tau_{\mathrm{rec}}), \quad \Delta_{\mathrm{I}}^{(\mathrm{SW})}(\vec{k},\tau_0)=\int_0^{\tau_0}(\phi'+\psi'). \tag{A.45}$$

At smaller angular scales the finite thickness of the last scattering surface cannot be neglected anymore and the general expression for the $C\ell$ coefficients becomes then:

$$C_\ell = \frac{2}{\pi}\int k^3 d\ln k\, |\,\Delta_{\mathrm{I}\ell}(k,\tau_0)\,|^2, \tag{A.46}$$

where

$$\Delta_{\mathrm{I}\ell}(k,\tau_0) = \mathcal{K}(\tau_{\mathrm{rec}})\left[(\Delta_{\mathrm{I}0}+\phi)_{\tau_{\mathrm{rec}}}\, j_\ell(x_0)+iv_{\mathrm{b}}\frac{dj_\ell(x_0)}{dx_0}\right]. \tag{A.47}$$

In Eq. (A.47) we the visibility function is approximated by a Gaussian in a way similar to what has been done in [39-41,45]:

$$\mathcal{K}(\tau_{\mathrm{rec}})=e^{-\sigma^2\tau_{\mathrm{rec}}^2k^2}, \quad \sigma=\frac{1}{\alpha_1\mathcal{H}_{\mathrm{rec}}\tau_{\mathrm{rec}}}=0.0148\left(\frac{\sqrt{z_{\mathrm{rec}}+z_{\mathrm{eq}}}+\sqrt{z_{\mathrm{rec}}}}{\sqrt{z_{\mathrm{rec}}+z_{\mathrm{eq}}}}\right) \tag{A.48}$$

where $\alpha_1 = 33.59$.

Note

[1]e-mail address: massimo.giovannini@cern.ch

[2]The terminology adiabatic (and non-adiabatic) is used to classify the initial conditions of curvature perturbations in the pre-equality plasma. A solution is said to be adiabatic if the fluctuations of the specific entropy vanish at large length-scales. The opposite is true for a non-adiabatic solution. See section 3 and discussions therein.

[3]In the present paper by B_{L} we denote the magnetic field smoothed over a typical comoving scale L = $2\pi/k_{\mathrm{L}}$ with k_{L} = Mpc^{-1}. This choice is purely conventional and refers to the occurrence that the gravitational collapse of the protogalaxy occurs over a typical comoving scale of the Mpc. The usefulness of this convention will become clear later on.

[4]As the name of the instrument suggests the collecting area of SKA will be of 10^6 m^2. The angular resolution of SKA is designed to be of 0.1 arcsec at 1.4 GHz. The frequency capability of the instrument will presumably be between 0.1 and 25 GHz. While the frequency range may be optimistic, it is certainly inspiring to think that 25 GHz is not so far from the 30 GHz of the low-frequency channel of the PLANCK Explorer [25]. This occurrence might have a relevant experimental impact for the possible analysis of Faraday rotated CMB polarization, as recently emphasized [27].

[5]The breaking of parity (often related to the turbulent nature of the bulk velocity field) is one of the necessary conditions for the persistence of the dynamo term in the magnetic diffusivity equation. For some classic introductions to

dynamo theory see [49,50]. In this paper it will be assumed that the pre-recombination plasma is not kinetically turbulent since the values of the kinetic Reynolds number drops below 1 for temperature smaller than the threshold of electron-positron annihilation [15]. Possible effects related to kinetic turbulence have been contemplated by the literature but for much higher temperatures in the life of the Universe but anyway always above the threshold of electron-positron annihilation (i.e. $T >$ MeV).

[6]For the Fourier transforms we use the following conventions: $B_i(\vec{x}) = (2\pi)^{-3/2} \int d^3k e^{-i\vec{k}\cdot\vec{x}} B_i(\vec{k})$ and, conversely, $B_i(\vec{k}) = (2\pi)^{-3/2} \int d^3x e^{-i\vec{k}\cdot\vec{x}} B_i(\vec{x})$.

[7]In the present and in the following sections the we we will often pass from the real space to the Fourier space description. We will avoid, though, to write the explicit subscripts referring to the Fourier mode since they might get confused with the indices labeling the fluctuations of the different species of the plasma.

[8]In Eq. (3.10) R_γ denotes the fraction of photons in the radiation plasma. Neutrinos are effectively massless prior to equality and their fraction will be denoted by R_ν. Note that $R_\gamma + R_\nu = 1$ and $R_\nu = r/(r + 1)$ where $r = 0.681(N_\nu/3)$. Consequently $R_\gamma = 0.594$ for three families, i.e. $N_\nu = 3$.

[9]Notice, incidentally, that nearly scale-invariant magnetic energy spectra also arise in string inspired cosmological models [56] as a consequence of the breaking of conformal invariance during the pre-big bang phase.

[10]The analytical calculation of the integral of Eq. (3.37) holds for $-3 < n_\zeta < 3$ and for $\ell < 30$. This means that the result is accurate for sufficiently large angular scale. In fact, the angular separation ϑ is approximately equal to π/ℓ. If $\ell < 26$, then $\theta > 7$ deg. This was, for instance, the region explored by the COBE team and it is the regime where CMB anisotropies computations may be usefully normalized.

[11]In section 5 the scalar spectral index will be denoted by n_ζ, stressing, in this way, that we refer to the spectral index appearing in the power spectrum of ζ.

[12]Notice that, in this paper, the natural logarithm will be denoted by ln while the base-10 logarithms will be denoted by log.

[13]In particular the data of the Supernova Legacy Survey (SNLS) [68] and the so-called Supernova "Gold Sample" (SNGS) [69,70].

[14]The values quoted for all the cosmological observables always refer to the case of a spatially flat Universe where the semi-analytical calculation has been performed.

[15]In the conformally flat parametrization adopted in the present paper (see also Eq. (2.1)), $\nabla^2 = \partial_i \partial^i$ is just the conventional Laplacian. If the spatial geometry would be curved, ∇^2 will be defined in terms of the appropriate spatial geometry. The analysis of open or closed Universes is, however, not central for the present analysis (see first and second paragraph of section 2). Notice, furthermore, that, as in the bulk of the paper, the prime denotes a derivation with respect to the conformal time coordinate τ.

References

1. Spergel DN, *et al.*: **[WMAP Collaboration].** . arXiv:astro-ph/0603449
2. Page L, *et al.*: **[WMAP Collaboration].** . arXiv:astro-ph/0603450
3. Peiris HV, *et al.*: **[WMAP Collaboration].** *Astrophys J Suppl* 2003, **148:**213.
4. Spergel DN, *et al.*: **[WMAP Collaboration].** *Astrophys J Suppl* 2003, **148:**175.
5. Bennett CL, *et al.*: **[WMAP Collaboration].** *Astrophys J Suppl* 2003, **148:**1.
6. Keskitalo R, Kurki-Suonio H, Muhonen V, Valiviita J: . arXiv:astro-ph/0611917

7. Kurki-Suonio H, Muhonen V, Valiviita J: *Phys Rev D* 2005, **71:**063005.
8. Enqvist K, Kurki-Suonio H: *Phys Rev D* 2000, **61:**043002.
9. Collins H, Holman R: . arXiv:0705.4666 [hep-ph]
10. Boyanovsky D, de Vega HJ, Sanchez NG: *Phys Rev D* 2006, **74:**123006.
11. Boyanovsky D, de Vega HJ, Sanchez NG: *Phys Rev D* 2006, **74:**123007.
12. Collins H, Holman R: *Phys Rev D* 2006, **74:**045009.
13. Giovannini M: **CERN-PH-TH-2007-048.** . arXiv:astro-ph/0703730
14. Carilli CL, Taylor GB: *Ann Rev Astron Astrophys* 2002, **40:**319.
15. Giovannini M: *Int J Mod Phys D* 2004, **13:**391.
16. Beck R, Brandenburg A, Moss D, Shukurov A, Sokoloff D: *Ann Rev Astron Astrophys* 1996, **34:**155.
17. Xu Y, Kronberg PP, Habib S, Dufton QW: *Astrophys J* 2006, **637:**19.
18. PP Kronberg: *Rep Prog Phys* 1994, **57:**325.
19. MJ Rees: *Lect Notes Phys* **664:**1.
20. A Brandenburg, K Subramanian: *Phys Rep* 2005, **417:**1.
21. Kulsrud R: *Ann Rev Astron Astrophys* 1999, **37:**37.
22. Harrison E: *Phys Rev Lett* 1967, **18:**1011.
23. Harrison E: *Phys Rev* 1968, **167:**1170. *Mon Not R Astr Soc* **147:279** 1970
24. Harrison E: *Rev Mod Phys* 1967, **39:**862.
25. **See, for instance** [http://www.rssd.esa.int/index.php?project=PLANCK]
26. Gaensler B, Beck R, Feretti L: *New Astron Rev* 2004, **48:**1003.
27. Giovannini M: *Class Quant Grav* 2006, **23:**R1.
28. Subramanian K, Barrow JD: *Phys Rev Lett* 1998, **81:**3575.
29. Subramanian K, Barrow JD: *Mon Not Roy Astron Soc* 2002, **335:**L57.
30. Mack A, Kahniashvili T, Kosowsky A: *Phys Rev D* 2002, **65:**123004.
31. Kahniashvili T: *New Astron Rev* 2005, **49:**79.
32. Tsagas CG, Barrow JD: *Class Quant Grav* 1997, **14:**2539.
33. Tsagas CG, Barrow JD: *Class Quant Grav* 1998, **15:**3523.
34. Giovannini M: *Phys Rev D* 2006, **73:**101302.
35. Giovannini M: *Phys Rev D* 2006, **74:**063002.
36. Giovannini M: *Class Quant Grav* 2006, **23:**4991.
37. Kahniashvili T, Ratra B: *Phys Rev D* 2007, **75:**023002.
38. Barrow JD, Maartens R, Tsagas CG: . arXiv:astro-ph/0611537
39. Jorgensen H, Kotok E, Naselsky P, Novikov I: *Astron Astrophys* 1995, **294:**639.
40. Naselsky P, Novikov I: *Astrophys J* 1993, **413:**14.
41. Seljak U: *Astrophys J* 1994, **435:**L87.
42. Hu W, Sugiyama N: *Astrophys J* 1995, **444:**489.
43. Hu W, Sugiyama N: *Astrophys J* 1996, **471:**542.
44. Weinberg S: *Phys Rev D* 2001, **64:**123511. ibid. 64 123512. 2001
45. Mukhanov VF: *Int J Theor Phys* 2004, **43:**623.
46. Krall NA, Trivelpiece AW: *Principles of Plasma Physics* San Francisco Press, San Francisco; 1986.
47. Biskamp D: *Non-linear Magnetohydrodynamics* Cambridge University Press, Cambridge; 1994.
48. Giovannini M: *Phys Rev D* 2005, **71:**021301.
49. Parker EN: Cosmical Magnetic Fields Clarendon Press, Oxford; 1979.

50. Zeldovich Ya B, Ruzmaikin AA, Sokoloff DD: *Magnetic Fields in Astrophysics* Gordon and Breach Science, New York; 1983.
51. Giovannini M: *Phys Rev D* 2000, **61:**063004.
52. Abramowitz M, Stegun IA: *Handbook of Mathematical Functions* Dover, New York; 1972.
53. Gradshteyn IS, Ryzhik IM: *Tables of Integrals, Series and Products* 5th edition. Academic Press, New York; 1994.
54. Kahniashvili T, Ratra B: *Phys Rev D* 2005, **71:**103006.
55. Subramanian K, Barrow JD: *Phys Rev D* 1998, **58:**083502.
56. Gasperini M, Giovannini M, Veneziano G: *Phys Rev Lett* 1995, **75:**3796.
57. Bardeen JM, Bond JR, Kaiser N, Szalay AS: *Astrophys J* 1986, **304:**15.
58. Cole S, *et al.*: **[The 2dFGRS Collaboration].** *Mon Not Roy Astron Soc* 2005, **362:**505.
59. Montroy TE, *et al.*: *Astrophys J* 2006, **647:**813.
60. Kuo CI, *et al.*: **[ACBAR collaboration].** *Astrophys J* 2004, **600:**32.
61. Readhead ACS, *et al.*: *Astrophys J* 2004, **609:**498.
62. Dickinson C, *et al.*: *Mon Not Roy Astron Soc* 2004, **353:**732.
63. Freedman WL, *et al.*: *Astrophys J* 2001, **553:**47.
64. Eisenstein DJ, *et al.*: **[SDSS Collaboration].** *Astrophys J* 2005, **633:**560.
65. Tegmark M, *et al.*: **[SDSS Collaboration].** *Astrophys J* 2004, **606:**702.
66. Semboloni E, *et al.*: . arXiv:astro-ph/0511090
67. Hoekstra H, *et al.*: *Astrophys J* 2006, **647:**116.
68. Astier P, *et al.*: **[The SNLS Collaboration].** *Astron Astrophys* 2006, **447:**31.
69. Riess AG, *et al.*: **[Supernova Search Team Collaboration].** *Astrophys J* 2004, **607:**665.
70. Barris BJ, *et al.*: *Astrophys J* 2004, **602:**571.